DETECTION OF RESPIRATORY SYNCYTIAL VIRUS DNA WITH GOLD NANOROD SURFACE ENHANCED RAMAN SPECTROSCOPY ACTIVE SUBSTRATES

A Thesis
Presented to
The Academic Faculty

by

Katherine Siemens

In Partial Fulfillment
Of the Requirements for the Degree
B.S. Chemistry with Research Option
in the School of Chemistry and Biochemistry

Georgia Institute of Technology

May, 2009

EPIGRAPH

"God made the bulk; surfaces were invented by the Devil."
~ Dr. Wolfgang Pauli

ACKNOWLEDGMENTS

I would like to thank Dr. Lawrence Bottomley and Nicole Marotta as well as the rest of the members of the Bottomley research group for their guidance and mentoring of my research.

TABLE OF CONTENTS

LIST OF FIGURES

LIST OF SYMBOLS AND ABREVIATIONS

IR	infrared (spectroscopy)
ν	wavenumber (cm^{-1})
λ	wavelength (nm)
SERS	surface enhanced Raman spectroscopy
GLAD	glancing angle deposition
AgNR	silver nanorod
n	nano
PCR	polymerase chain reaction
AuNP	gold nanparticle
DNA	deoxyribonucleic acid
RSV	respiratory syncytial virus
RNA	ribonucleic acid
R6G	rhodamine 6G
ssDNA	single-stranded DNA
M	molar (mol/L)
AuNR	gold nanorod
Å	angstrom
SEM	scanning electron microscope (microscopy)
μ	micro
m	milli
SEF	surface enhancement factor

SUMMARY

Surface enhanced Raman scattering (SERS) is a powerful spectroscopic tool that can be used to identify and characterize compounds at low concentrations. Recent literature reports suggest that SERS may be applicable for the detection and identification of viruses present in biofluids. In this investigation, gold nanorod arrays were evaluated as SERS substrates with the specific purpose of probing spectral differences between single stranded (ssDNA) and hybridized, or double stranded (dsDNA) DNA. This was deemed as the first step in developing a SERS-based hybridization assay for viral identification. Hybridization was carried out both off and on the substrate surface to determine whether there are observable spectral differences from the two different methods of hybridization. Studies were also carried out to determine if it was possible to detect mismatched DNA pairs after hybridization had been attempted.

Gold SERS active substrates were utilized instead of silver giving the advantage that these substrate do not oxidize under ambient conditions. It has also been found that ozone cleaning gold substrates before sample application increases the hydrophilicity of the gold, making the use of smaller sample volumes possible. Ozone cleaning the gold substrate after ample binding time has passed increases the SERS signal as well. It is believed that this cleaning immediately prior to SERS acquisition cleans the gold surface to a point where the plasmon being formed is more likely to move up the sample which increases the intensity of the SERS signal.

In addition to examining the possibility of using gold instead of silver for the SERS substrates, a method allowing for 36 separate DNA assays to be run at one time was investigated. This is accomplished by creating wells with polymer. Up to 36 wells fit on one glass microscope slide meaning that anywhere from 1 to 36 DNA probes can be attached within individual wells. This allows for either 36 different biological assays for the same virus or 1 biological sample to be tested for 36 different viruses or virus strains.

CHAPTER 1

INTRODUCTION

Surface Enhanced Raman Spectroscopy

Raman spectroscopy is a technique that was discovered by Raman in 1928 [Raman, 1928] and developed by Raman and Krishnan [Raman and Krishnan, 1928] to measure the light scattered from molecules that is either lower or higher in energy than the incident beam of light. Raman is complementary to infrared spectroscopy in that the spectral lines correspond to vibrational modes of bonds within the molecule; it is dependent upon a net change in polarizability rather than a change in dipole moment. [McCreery, 2000; Skoog, 2007] The change in dipole necessary for infrared spectroscopy occurs from a shift in electron density within the molecule during the vibration. The polarization necessary for Raman spectroscopy arises from a momentary distortion of the electron distribution surrounding a bond. [Skoog, 2007]

Light scatters whenever it interacts with matter. The majority of the light is reflected back at the same wavelength (Rayleigh scattering). A smaller portion of the light is scattered at either a lower or higher energy than the incident light (Stokes and anti-Stokes scattering, respectively). With Stokes and anti-Stokes scattering, the electrons are excited into a virtual state. This virtual state, however, is not a true quantum state; rather this virtual state can be regarded as a momentary distortion in the electron distribution. The distortion is caused by the oscillating electric field of the incident light. [McCreery, 2000] (Figure 1)

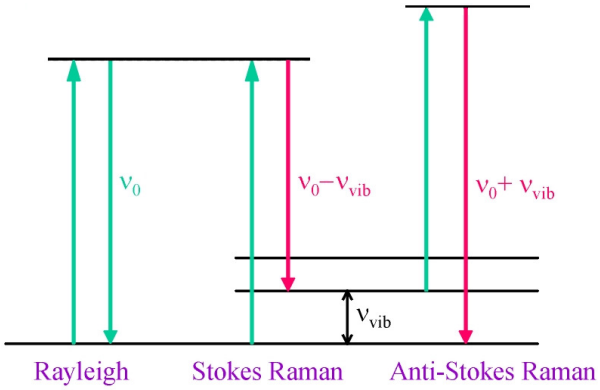

Figure 1: **Diagram of Light Scattering Events**. Raman spectroscopy measures the Stokes and anti-Stokes shifts. Most commonly, only the Stokes shifts are reported as they are significantly higher in intensity than the corresponding anti-Stokes shifts. [http://www.vub.ac.be/META/toestellen_raman.php?m=xpand&d=menu7] Adapted without permission.

Raman spectroscopy has many advantages over infrared (IR) spectroscopy. One of the biggest advantages is that water and other polar solvents can be used because they do not appear in Raman spectra. [Skoog, 2007] Additionally, because Raman spectroscopy most commonly utilizes light sources in the visible and near-IR range, glass and quartz sample holders can be used as opposed to the occasionally atmospherically unstable window materials (i.e. sodium chloride (NaCl) or potassium bromide (KBr)) necessary for IR measurements. [Skoog, 2007] Limitations to Raman spectroscopy include the need for bulk analyte and interference of sample fluorescence. Also, as only a miniscule amount of the incident light experiences Stokes and anti-Stokes scattering, there are problems with insufficient light collection.

While the observed Raman shift is independent of the wavelength of the incident light, the actual bands do show wavelength dependence. Equation 1 shows how the Raman shift is calculated.

$$\Delta\nu = \frac{1}{\lambda_I} - \frac{1}{\lambda_O} \qquad \text{Equation 1}$$

Where $\Delta\upsilon$ is the observed Raman shift, λ_I is the wavelength of the incident light and λ_O is the wavelength of the observed spectral band. The greater the wavelength (lower energy) of the incident beam of light, the larger the shift in wavelength will be. This means that lower energy light sources will show a greater wavelength shift in the scattered light. There is, however, no change in the energy (wavenumber) shift. [Strobel, 1973]

The advent of Fourier transform (FT) Raman resolved the many of the issues of traditional Raman spectroscopy making chemical analysis possible. [McCreery, 2000] Fourier transform Raman spectrophotometers use an interferometer and a continuous wave laser emitting at a wavelength of 1064 nm. This setup greatly diminishes fluorescence or photodecomposition of samples as the laser is not high enough in energy to cause the electronic state transitions necessary for the occurrence of fluorescence. [Chase, 1994] The superior frequency precision allows for high-resolution measurements to be made. [Chase, 1994; Skoog, 2007]

The phenomenon of surface enhanced Raman spectroscopy (SERS) was discovered independently by two groups: Albrecht and Creighton [Albrecht, 1977] and Jeanmarie and Van Duyne. [Jeanmarie, 1977] Fleishmann *et.al*. actually reported data in 1974 that demonstrated the SERS effect, [Fleischmann, 1974] however, it wasn't until the work was repeated in 1977 that the phenomenon was actually reported. SERS allows for higher spectral counts from smaller sample sizes.

Many theories have been put forth since the discovery of SERS in 1977 as to the actual mechanism(s) that gives rise to the enhanced signal. The overall enhancement has both chemical and electromagnetic components. [Arunkumar, 1983; Gersten, 1980; Kim, 2003; King, 1978] It is generally accepted now that the electromagnetic component

of the enhancement is due to an interaction between the substrate surface plasmon and the analyte. [Arunkumar, 1983; Kim, 2003; King, 1978; McCall, 1980] The chemical enhancement is said to come from scattering processes associated with the chemical interactions between the analyte and the substrate surface (*i.e*. adsorption). [Kim, 2003; Vo-Dinh, 1999]

A requirement of this technique is a SERS active substrate. [King, 1978] This is achieved using coinage metals due to their ability to support surface plasmons allowing amplification of the signal. With the increased sensitivity of the SERS method, it is possible to detect micromolar concentrations of samples accurately and reproducibly. [Moskovits, 1985] Not all coinage metals give the same enhancement. Silver gives a significantly higher surface enhancement than gold due to the reduced reflectivity of gold in the visible region. [Arunkumar, 1983]

There are multiple methods by which a SERS active substrate can be achieved. Some of the most common SERS active substrates are roughened electrodes, island films, metal-coated nanospheres, metal-coated nanostructures, metal nanoparticles-embedded polymers and other metallic nanostructures. [Driskell, 2008A; Driskell, 2008B; Gish, 2007; Martinez, 1986; Vo-Dinh, 1999] The substrate selected depends on the needs of the experimenter. Aligned nanorod arrays have been shown to give reproducible SERS signal enhancement. [Driskell, 2008B]

Glancing Angle Deposition

The morphology of the SERS active substrate plays a large role in the sensitivity and the intensity of the Raman bands. Glancing angle deposition (GLAD) is a technique used to fabricate aligned microstructures. [Robbie, 1998] The substrate is held at an angle

above the plume of vaporized metal being deposited. The angle at which the substrate is held determines the angle of growth from normal on the substrate. [Robbie, 1998] (Figure 2) Researchers have used GLAD to fabricate silver nanorod (AgNR) arrays that are SERS active. The length of the AgNRs increase proportionally with the time the slide is exposed to the silver plume. [Chaney, 2005]

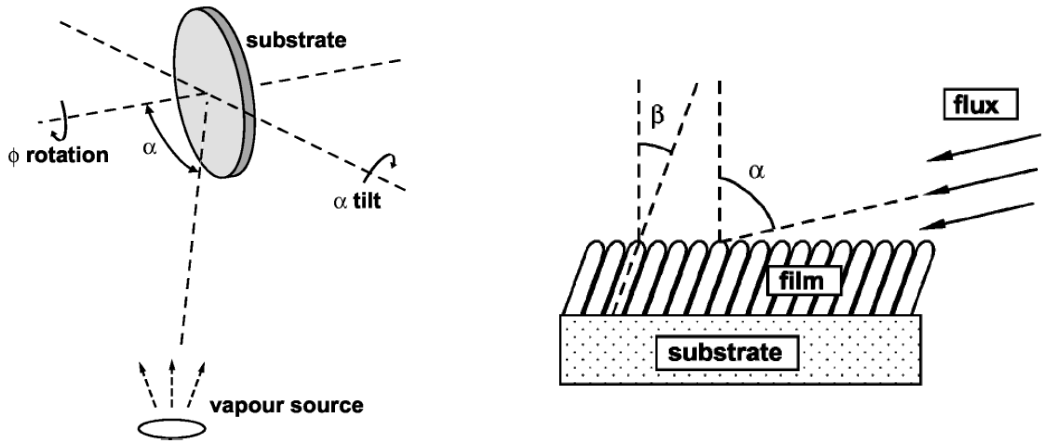

Figure 2: **Traditional GLAD Setup Schematic and Diagram of Nanorods Produced**. The flux angle (α) is the angle of incident flux material. The growth angle (β) is the angle at which the column deviates from normal. [Robbie, 1998] Reproduced without permission.

Because nanorod arrays are being investigated as potential biosensing SERS substrates, a high level of reproducibility in signal enhancement is crucial. A study has been performed to investigate the potential of aligned AgNRs arrays as SERS active substrates. [Driskell, 2008B] The overreaching goal of that study was to determine if aligned silver nanorod arrays produced via the GLAD method gave a reproducibly high surface enhancement. It was also a goal of this study to determine what size nanorod gave the best enhancement. Two different methods were used to fabricate substrates. Some silver nanorods were grown directly onto a glass slide, while others were grown on a 500 nm layer of silver deposited at normal incidence. These methods served to

compare the potential difference in nanostructure morphology and to see if one gave better enhancement than the other. [Driskell, 2008B]

For the study of the effect of nanorod length, it was reported that the optimum SERS enhancement was found at a nanorod length of 868 nm with 785 nm incident light. The observation that nanorods on the 500 nm layer of silver resulted in better enhancements than nanorods grown directly on glass was attributed to the capability of the surface plasmon to not only interact with the rods, but with the silver underlayer as well. [Driskell, 2008B] As for reproducibility, it was found that the SERS responses from substrates fabricated within the same batch varied by only 6-13% and the signal variance between batches was ~15%. [Driskell, 2008B]

The magnitude of the enhancement varies with either the type of roughened surface or the morphology of the nanostructures on the surface of the substrate. AgNRs are uniform, reproducible structures that exhibit very high signal amplification factors (10^8). In addition to being inexpensive to fabricate, silver nanorods possess a large surface area for plasmon interaction and provide a highly reproducible response. [Shanmukh, 2006]

Bioapplications of SERS

The current methods for the biological testing for microorganismal infection rely on polymerase chain reaction (PCR) amplification and the use of fluorophores as labels. While these methods have picomolar detection limits, many drawbacks remain. The selective target amplification of PCR can lead to distorted gene expression and the fluorophores experience problems with non-uniform photobleaching. [Tansil, 2006] The use of gold nanoparticles (AuNPs) modified with oliogonucleotide detection probes for

deoxyribonucleic acid (DNA) analysis has shown to be a viable detection method. The AuNPs serve as a good alternative to fluorophore labeling due to the amplified Raman signal (SERS effect) and the narrow spectral characteristics that are found. The use of the AuNPs also eliminates photobleaching problems. [Tansil, 2006]

SERS has also been shown to be useful in biomedical diagnostics and genomic analysis. The hybridization of nucleic acids to DNA biotargets has been shown to give a high degree of accuracy in the identification of DNA sequences which are complimentary to the probe. [Vo-Dinh, 1999] The use of SERS active labels which are compatible with the hybridization platforms being employed have shown promise in replacing radioactive labels and luminescent labels which have poor spectral specificity. [Vo-Dinh, 1999]

Biosensors have been developed from silver nanostructures fabricated by the GLAD method. The biosensors fabricated were used in surface plasmon resonance (SPR) measurements and were found to increase the local refractive index and red-shift the extinction peak. [Gish, 2007] The GLAD method was specifically chosen for the biosensor fabrication because it allowed the researchers the ability to easily control the density of the film. [Gish, 2007] The ability to differentiate molecular fingerprints for multiple pathogens using nanorod arrays produced via GLAD has also been reported. [Driskell, 2008A] For SERS applications in biosensing, the SERS substrates must have highly reproducible structures and an easily controlled protrusion size. [Vo-Dinh, 1999] Nanorod arrays produced via the GLAD technique have been shown to have high levels of reproducibility, not only within a fabrication batch but also between fabrication batches. [Driskell, 2008A; Driskell, 2008B]

Viral Sensing with SERS

The development of a SERS based assay using silver nanorods that allow for detection of trace levels of viruses with high selectivity has been reported. [Driskell, 2008A; Shanmukh, 2008; Shanmukh, 2006] This method allows for rapid detection and identification of both virus type and strain without manipulation of the virus. The ability to detect gene deletions in complex biological media has also been found. [Shanmukh, 2006]

Currently employed methods for viral detection suffer from poor sensitivity of the rapid antigen testing method as well as a delay in results from traditional viral cultures. Cases have been reported where rapid antigen testing of patients with a known respiratory syncytial virus (RSV) infection gave negative results. [Caram, 2009] Immunofluorescence assays have also been used to detect viral infections; however, this method of diagnosis is often performed retrospectively. [Caram, 2009]

RSV is a negative sense, enveloped virus from the Paramyxoviridae family. There are only two subtypes to the RSV virus (A and B) and it is currently not clear whether or not one of these types is more virulent than the other. RSV is a major respiratory virus for all ages and is transmitted through respiratory secretions. Transmission can occur from contact with infected persons or through contact with a contaminated surface. [http://www.cdc.gov/ncidod/dvrd/revb/respiratory/rsvfeat.htm; Chávez-Bueno, 2005] It is estimated that all children in the United States have been infected with RSV by the age of 3. [Chávez-Bueno, 2005] Because there are only two strains of the RSV virus it is a relatively simple virus to work with when investigating viral identification methods.

In patients with a healthy immune system, RSV presents with symptoms similar to that of the common cold. However, in infants, the elderly and immunocompromised patients RSV can cause permanent respiratory tract damage and can even prove to be fatal. [http://www.cdc.gov/ncidod/dvrd/revb/respiratory/rsvfeat.htm; Chávez-Bueno, 2005] Work is currently being performed at the University of Georgia (UGA) to sense intact viruses with SERS. Further virus hybridization studies are being carried out at the Georgia Institute of Technology (Georgia Tech).

SERS of DNA

Since RSV is a ribonucleic acid (RNA) virus, detection requires the ability of distinguishing between single stranded DNA, hybridized DNA, RNA and DNA-RNA hybrids. [Fang, 2008; Mulvaney, 2000] SERS studies of the individual DNA components (Figure 3), including nucleotides, have been previously published. [Bell, 2006; Green, 2006; Otto 1986]

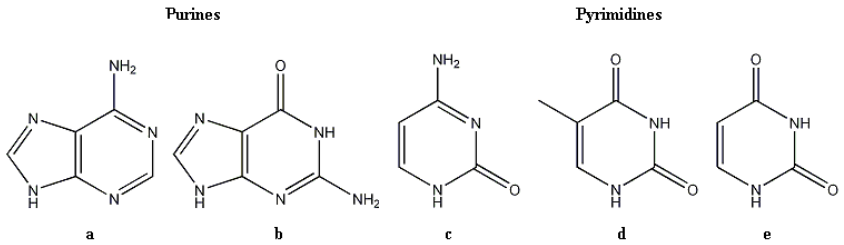

Figure 3: **Structures of the DNA and RNA Nucleotides**. (a) adenine (b) guanine (c) cytosine (d) thymine (e) uracil

The spectra of the nucleotides are rich in vibrations associated with the bases; minimal spectral components are observed from the sugar and phosphate groups in the backbone. [Green, 2006] Spectra were presented along with an analysis of the bond vibrations, stretching and bending that gave rise to each of the spectral peaks. It was determined that bases chemisorbed onto a silver surface gave significantly higher intensities when

compared to intensities from DNA nucleotides in solution. This is due to the added chemical enhancement from the adsorption to the metal surface. Without this adsorption, there is only an electromagnetic enhancement. It is now known that with the silver surfaces, a plasmon effect is responsible for the enhancement seen in the SERS spectra. [Otto, 1986]

Project Goals

There were five main goals for this project. The first was to fabricate gold nanorod arrays using oblique angle deposition and pattern substrates with the method developed by Marotta *et.al*. [Marotta, in progress] The achievement of this goal was necessary for any further work to be completed and this goal was achieved early on in the project. The second goal of the project was to determine the surface enhancement factor using rhodamine 6G (R6G) dye. This determination allowed for the comparison of the gold substrates to the silver substrates also being investigated. Once the gold enhancement factor was determined the next goal was to evaluate the immobilization of single stranded DNA (ssDNA), through a thiol group, to the substrate surface. After the ssDNA immobilization was evaluated, the goal was to evaluate the hybridization of DNA on a SERS substrate. The final goal of the research was to develop a gold nanorod array specifically for the detection of RSV.

CHAPTER 2

EXPERIMENTAL METHODS

Materials

The R6G dye used as a probe analyte was obtained from Tokyo Chemical Industry (TCI) and solutions were made in nanopure water unless otherwise specified. The R6G solutions were kept out of direct light to avoid photo degradation of the dye. The thiols used in the early studies were obtained from Sigma-Aldrich and all solutions were made in nanopure water and had a concentration of 10^{-5} M unless otherwise specified.

The RSV oligos were obtained from IDTDNA and The Midland Certified Reagent Company and were used without further purification. The stock solutions were diluted to a concentration of 10^{-5} M for use in these studies. The RSV oligos found in Figure 4 were used in the experiments outlined below.

Figure 4: **Sequences of RSV DNA Oligos Used**. The odd numbered oligos were the probe strands and the even numbered oligos were their compliments. As can be seen RSV3 and RSV11 have the same sequence of nucleotide residues with differing 5' end groups.

Ologo	Sequence (ssDNA)	Additional Information
RSV 1	5'-thiol-GCATTCATAAACAATCCTGCA-3'	Probe – 1
RSV 2	5'-TGCAGGATTGTTTATGAATGC-3'	Compliment – 1
RSV 3	5'-thiol-CTTCATTGTTATCAAATGTTTC-3'	Probe – 2
RSV 4	5'-GAAACATTTGATAACAATGAAG-3'	Compliment – 2
RSV 5	5'-thiol-TGCAGTATCATCTGTCTC-3'	Probe – 3, Strain A
RSV 6	5'-GAGACAGATGATACTGCA-3'	Compliment – 3, Strain A
RSV 7	5'-thiol-TGGGGTACTGTCGGCTTC-3'	Probe – 4, Strain B
RSV 8	5'-GAAGCCGACAGTACCCCA-3'	Compliment – 4, Strain B
RSV 9	5'-thiol-AGCTCATCTTAAAGC-3'	Probe – 5
RSV 10	5'-GCTTTAAGATGAGCT-3'	Compliment – 5
RSV 11	5'-amine-CTTCATTGTTATCAAATGTTTC-3'	Probe – 2

Substrate Fabrication

The gold nanorod (AuNR) substrates were fabricated at Georgia Tech by Nicole Marotta using a modified GLAD scheme in a CVC electron beam (e-beam) evaporator. The rate of deposition was set to 3Å/sec and monitored with a quartz crystal microbalance located within the evaporation plume. The base pressure at the start of deposition was 10^6 torr. A hexagonal platen was used to enable the fabrication of six AuNR substrates at a time. The source metal was centered to create even particle density for all substrates as seen in Figure 5. The slides were held at an angle of 80.9° from normal in relation to the plume to achieve a flux angle of 86°. The nanorods produced were 400-500 nm in length. All substrates were stored in a desiccator at room temperature.

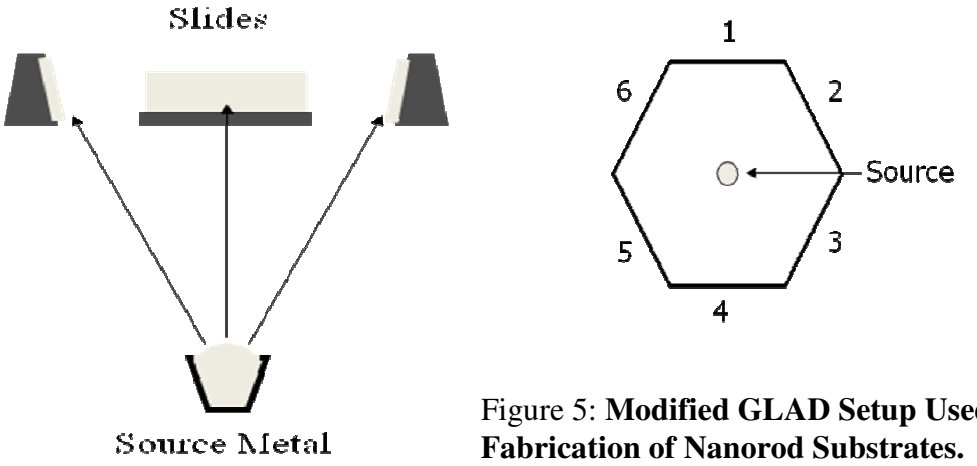

Figure 5: **Modified GLAD Setup Used for Fabrication of Nanorod Substrates.**

A UV curable polymer (Epotek, Epoxy G042) was contact printed onto each substrate to create 36 physically isolated wells using a custom made stamp. This allows for 36 assays to be run simultaneously without cross-contamination. Figure 6 shows a schematic of a stamped substrate with an image of a corner of a stamped substrate.

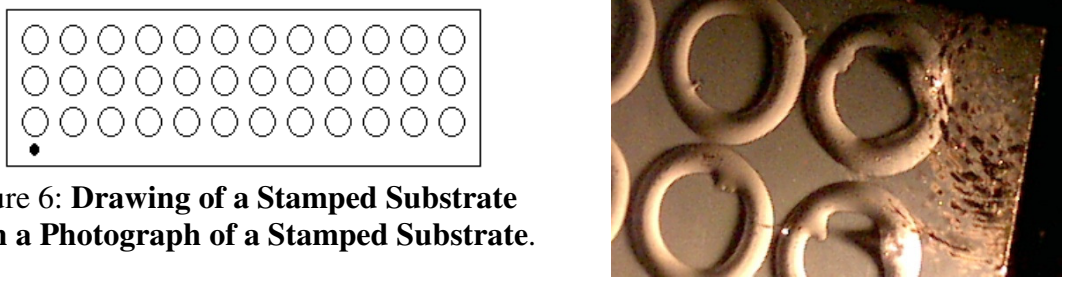

Figure 6: **Drawing of a Stamped Substrate with a Photograph of a Stamped Substrate**.

A Zeiss Ultra 60 scanning electron microscope (SEM) was used to confirm the formation of nanorods. The SEM measurements were carried out under in vacuum. The substrates were attached to the SEM holder with copper tape. The tilt angle in the SEM was set to 52° to facilitate the measurement of the nanorod length and angle. All other SEM images were taken at a tilt angle of 0°. Figure 7 shows a SEM image of AuNRs taken from above.

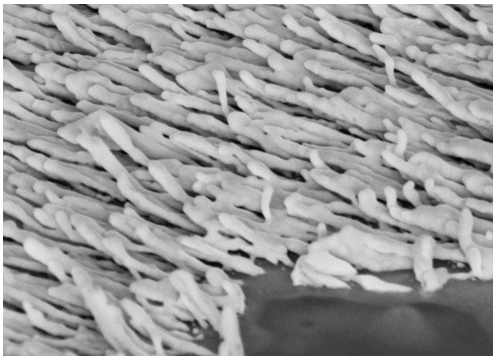

Figure 7: **SEM Image of AuNRs**.

All SERS measurements were made with a Kaiser Holoprobe using a 785 nm continuous wave helium/neon laser (HeNe) unless otherwise specified. The microscope used was incased in a black felt lined plastic enclosure to prevent interference from outside light. Any stray light was accounted for and subtracted from the spectra acquired. The spectra were taken at room temperature.

Rhodamine 6G Power Study

The effect of the power of the laser on the SERS signal was investigated by increasing the laser power and observing the changes in signal intensity. A silicon chip was used to calibrate the laser for each power at which spectra were taken. The power was adjusted so that the peak at 520 cm^{-1} on the silicon chip was approximately 1000 counts. A gold SERS substrate containing 10μL of a R6G solution evaporated in one of the wells was analyzed and five spectra were taken in this well to account for any variability in evaporation. The power of the laser was increased until the peak at 520 cm^{-1} on the silicon chip was approximately 1200 counts and the evaporated R6G was again analyzed. This process was repeated for laser powers of 1400, 1600, 1800, and 2000 counts. The surface power was measured with a power meter to determine the surface power associated with the laser power giving 1000 counts on silicon. A surface power of 4.5mW was determined to be best for measurements and was used in all future studies.

The distance dependence between the surface and the laser source was determined by focusing the substrate visually with a microscope and then acquiring spectra as the microscope stage was moved in 25μm increments in the z direction. For the remainder of the studies, the surface was visually focused and then the stage was moved down 200μm before spectra were acquired.

The surface enhancement factor (SEF) was calculated using the method described by Ru *et. al*. where I_{SERS} is the SERS intensity, N_{SERS} is the average number of adsorbed molecules in the scattering volume, I_{Raman} is the Raman intensity under the same conditions and N_{Raman} is the average number of molecules in the scattering volume. [Ru, 2007]

$$SEF = \frac{I_{SERS} / N_{SERS}}{I_{Raman} / N_{Raman}}$$ Equation 2

Spectra were acquired for bulk analyte as well as on the SERS AuNR substrate. Peak heights at 611, 771, 1311 and 1360 cm^{-1} were used to calculate the SEF.

Drying Pattern across a Well

A 10μL aliquot of R6G was pipetted into a well on a patterned AuNR substrate. The laser was focused on the polymer at one side of the well and spectra were obtained across the well in 25μm increments in the x direction. (Figure 8)

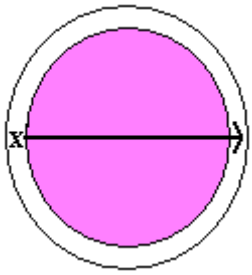

Figure 8: **Diagram of Movement Across the Well for the Drying Pattern Study**.

Ozone Cleaning Study and Volume Study

Both studies were carried out simultaneously on the same substrate. A glass slide was used to cover the first two rows of wells (Figure 9). The substrate was then placed in an ozone cleaner for ten minutes. Ozone cleaning is a method for cleaning a surface through oxidation with ozone. The sample is placed in a box and UV light is used to radicalize the oxygen from the air inside to generate the ozone.

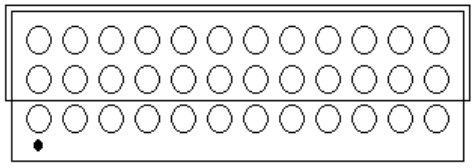

Figure 9: **Setup Used for Ozone Cleaning Study**.

The cover slide was removed at the completion of the ozone cleaning cycle. 15μL aliquots of solution were pipette into the wells in row A (Figure 10). 10μL aliquots of solution were pipette into each of the wells in rows B and C (Figure 10). The same solution was used in each of column of wells along the slide.

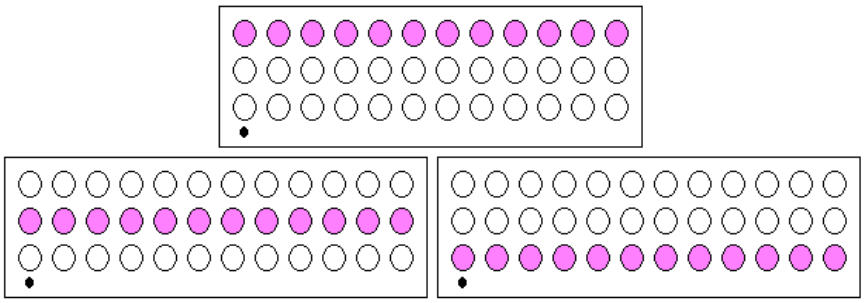

Figure 10: **Rows A, B and C on a Substrate**.

The solutions in the wells across each row were R6G, RSV1, RSV2, RSV3, RSV4, RSV5, RSV6, RSV7, RSV8, RSV9, RSV10 and RSV11. All solutions had concentrations of 10^{-5} M.

Thiol Studies

Solutions of 2-aminoethanethiol hydrochloride, benzyl mercaptan, 11-mercacpto-1-undecanol, 4-nitrobenzenethiol, 4-aminothiophenol and 4-mercaptobenzoic acid were analyzed on gold substrates. Studies were carried out using 4-nitrobenzenethiol, 4-aminothiophenol, 4-mercaptobenzoic acid, 4-methylbenzenethiol, 4-fluorobenzenethiol, 4-mercaptophenol and 4-methoxybenzenethiol. The benzenethiols solutions were made in both 1X SSC buffer and nanopure water to determine which gave the better signal. The benzenethiol pairs found in Figure 11 were used in ratiometric studies to investigate the potential for quantative analysis.

Figure 11: **Table of Benzenethiol Pairs Used in Ratiometric Study.**

Pair	Thiol 1	Thiol 2
1	4-methylbenzenethiol	4-mercaptobenzoic acid
2	4-mercaptobenzoic acid	4-mercaptophenol
3	4-nitrobenzenethiol	4-methylbenzenethiol
4	4-nitrobenzenethiol	4-mercaptobenzoic acid
5	4-nitrobenzenethiol	4-mercaptophenol

Spectra of Single-Stranded and Double-Stranded DNA Pairs

The characteristic SERS spectra of each of the four DNA bases (adenine, thiamine, guanine and cytosine) were obtained first. Spectra were taken of each of the RSV oligos being studied. Both 3' thiolated and non-thiolated oligos of RSV2, RSV4, RSV6, RSV8 and RSV10 were studied to determine how the strands were binding to the AuNR surface. For hybridization studies, 10μL of both the probe strand and the complement were pipetted into a micro centrifuge tube, heated and then cooled to allow for annealing of the two strands. Noncomplementary dsDNA was prepared in the same fashion.

CHAPTER 3

RESULTS AND DISCUSSION

Spectra Acquisition Optimization

Initial spectra were taken on the Kaiser Holoprobe system described above. R6G was examined on the AuNR substrates and the spectra were compared to those obtained on equivalent silver substrates. As can be seen in Figure 12, the AuNR substrates produce the same SERS signals as the AgNR substrates. The signal intensity obtained with the AuNRs was significantly less than that obtained with the AgNRs. Additionally, the signal to noise ratio is lower on the gold substrates than it is on the silver substrates.

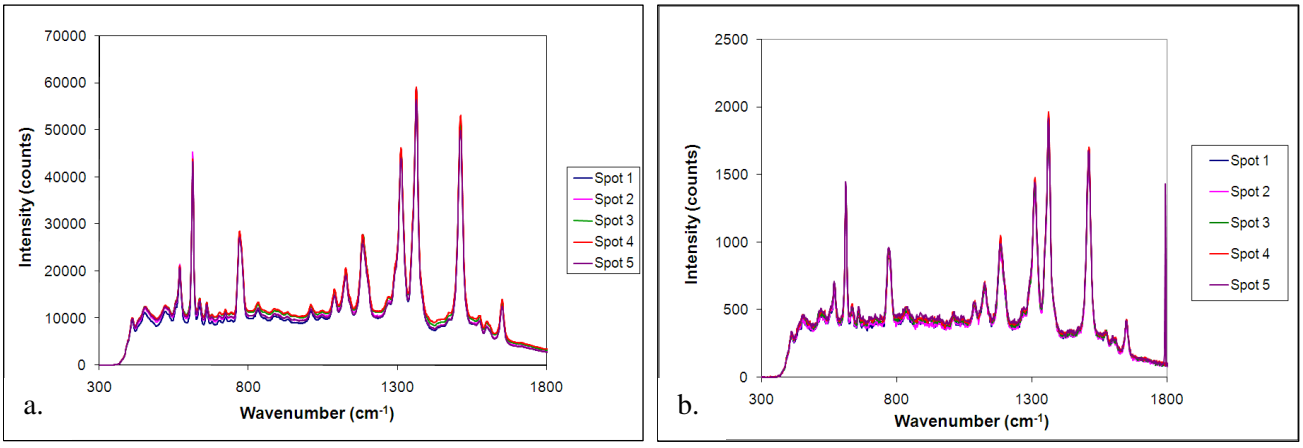

Figure 12: **R6G Spectra Taken on Silver (a) and Gold (b) Nanorods Arrays**.

The proper volume of DNA for studies as well as whether or not ozone cleaning of the substrates was necessary was determined from the ozone and volumetric study outlined above. Based on these results it was decided to proceed without ozone cleaning the substrates prior to sample deposition. Also it was decided to use a sample volume of 10µL for the remaining studies. Figure 14 shows the R6G spectra from the study; all of

the spectra from the study can be found in Appendix A. The surface enhancement on the AuNR substrates under these conditions can be found in Figure 13.

Figure 13: **Surface Enhancement Factors for AuNR substrates**.

Raman Shift (cm^{-1})	Enhancement
611	$7.24*10^4$
771	$8.11*10^4$
1311	$6.15*10^4$
1360	$4.83*10^4$

Figure 13 shows that all of the enhancements are on the order of 10^4. The bulk R6G solution had 26X more molecules excited than the solution from which the SERS measurement was made. This shows that AuNRs are a viable SERS substrate for analyte detection.

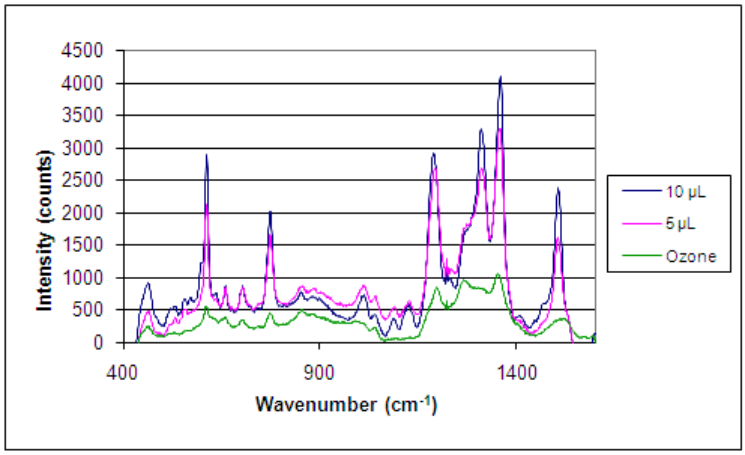

Figure 14: **SERS spectra of R6G from Ozone and Volume Study.** Sample volumes of both 5 and 10µL were examined as well as the effect of ozone cleaning of the substrate prior to sample deposition.

It was decided to investigate the possibility of using a different excitation wavelength to improve the SERS response on the gold substrates. It is well known that, though the Raman shift is not dependant on the excitation wavelength, there is still a spectral dependence on the excitation wavelength used. It was thought that a higher

energy (lower wavelength) laser might improve the SERS response on the AuNR substrates. A multiwavelength Renishaw Raman system (at the University of Georgia) was used to determine the optimum laser wavelength for future measurements. Lasers at 514 nm, 633 nm and 785 nm were all tested and the results can be seen in Figure 15. The counts from the 785 nm laser are over twice the intensity of the counts from the 633 nm laser. The 514 nm laser showed fluorescence rather than SERS.

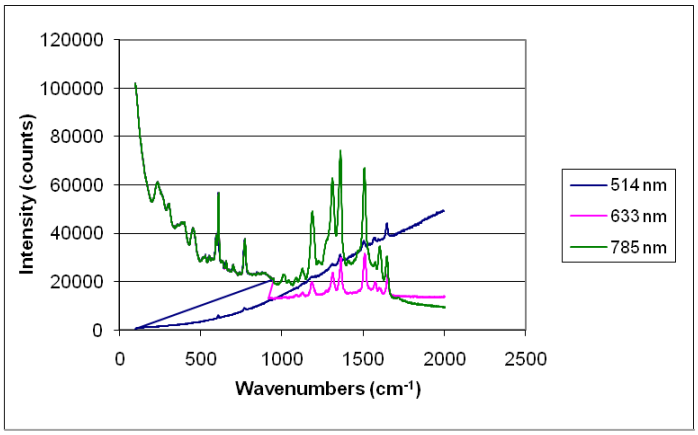

Figure 15: **Graph of Incident Wavelength Dependence**.
Comparison of R6G spectra taken with
514 nm, 633 nm and 785 nm lasers.

There was sufficient energy in the 514 nm laser to fully excite the electrons into an excited state from which they decayed and emitted a photon, namely they fluoresced. The fluorescence signal interfered with the Raman signal as fluorescence is a stronger effect than the light scattering that Raman measures. It is apparent from the graph in Figure 15 that a lower energy (higher wavelength) laser gives a better SERS response. A 785 nm laser was the lowest energy option available so it was decided to do all future studies with a 785 nm light source.

A positional analysis was done to study the signal reproducibility across a well. This was done in an effort to investigate whether the analyte spreads evenly across the

well surface. It was also done to investigate the claim that analyte molecules in close contact with multiple nanorods would create "hot spots" with a significantly increased signal intensity compared to the surrounding area. Spectra were taken in 25μm increments across a well containing 10μL of a R6G solution. The intensities of the peaks found at 611, 771, 1311 and 1360 cm^{-1} were graphed as a function of position across the well (Figure 16). The average, standard deviation, maximum and minimum for the linear region of the graph were found (Figure17).

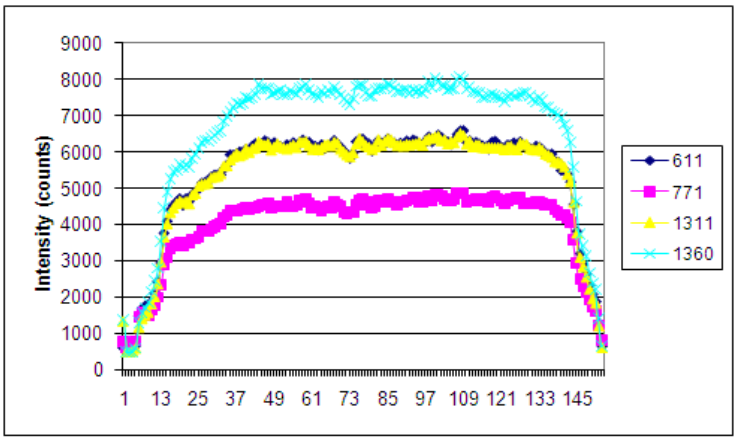

Figure 16: **SERS Intensity of R6G peaks across a Well.** The peaks at 611, 771, 1311 and 1360 cm^{-1} were analyzed.

Figure 17: **Statistical Values for the R6G Peaks Analyzed.** The Averages, Standard Deviations, Maxima, and Minima were calculated for each peak.

Wavenumber	Average	Standard Deviation	Maximum	Minimum
611	6239.7	124.59	6602.0	5834.5
771	4620.0	122.07	4878.3	4316.1
1311	6196.5	117.70	6510.0	5864.4
1360	7686.4	147.55	8079.9	7315.3

Thiol Studies

The technological applications of terminally-substituted alkanethiols chemisorbed onto metal surfaces (specifically gold, silver and copper) have been extensively investigated. [Jans, 2008; Kudelski, 2003; Maksymovych, 2008; Otto, 1986] The thiol

end (H-S group) binds strongly to the metal substrates and forms a highly stable metal-sulfur bond. The functional group on the opposite end of the alkanethiol is left free to participate in other chemical processes making these species good binding agents. [Kudelski, 2003]

Thiols are well known to form self-assembled monolayers (SAMs) on metal surfaces. It is also known that the functional group on the thiol influences the properties of the SAMs and can affect the monolayer structure. [Kim, 2003; Kudelski, 2003] It has been shown that the angle between the functional group and the surface in smaller for gold-sulfur bonds than it is for silver-sulfur bonds. This allows for increased interaction between the functional group and the metal surface. While this increased interaction can hinder the thiol's ability to act as a linker between the metal surface and an analyte, the proximity of the functional group to the surface may improve the signal strength on the gold substrate over the signal if the angle between the functional group and the substrate were larger. [Kudelski, 2003]

SERS spectra of 2-aminoethanethiol hydrochloride, benzyl mercaptan, 11-mercacpto-1-undecanol, 4-nitrobenzenethiol, 4-aminothiophenol and 4-mercaptobenzoic acid were taken to determine which gave the strongest signal. It was found that 4-nitrobenzenethiol, 4-aminothiophenol and 4-mercaptobenzoic acid gave the best response and were used for the remainder of the thiol studies. Additionally, 4-methylbenzenethiol, 4-fluorobenzenethiol, 4-mercaptophenol and 4-methoxybenzenethiol solutions were made and spectra taken.

The benzenethiol solutions were made in both 1X SSC buffer and nanopure water to determine which gave the better signal. As can be seen in Figure 18, the spectra taken

in wells containing buffer had a lower signal to noise ratio than those acquired in wells containing water. Also, the salt in the buffer crystallized and the crystals interfered with the SERS response due to the increased light scattering from the irregular crystalline surface.

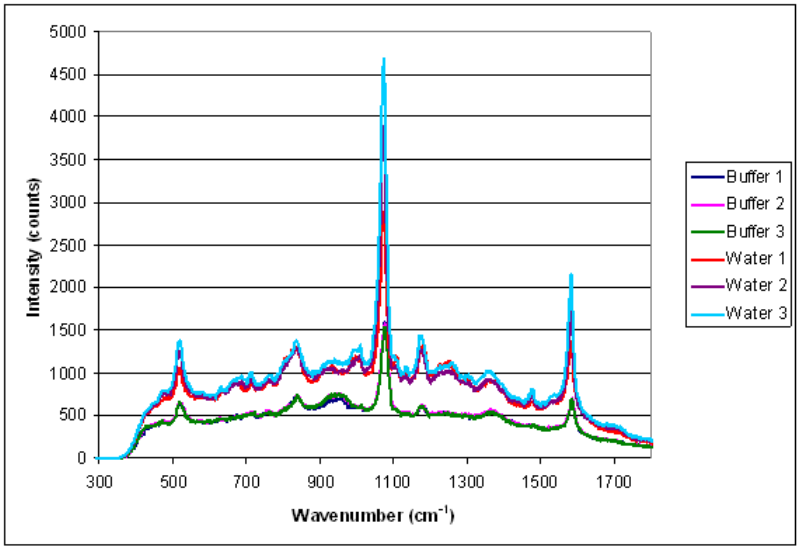

Figure 18: **Comparison of 4-Mercaptobenzoic Acid Spectra**. 3 wells contained the thiol dissolved in buffer and 3 wells contained the thiol dissolved in water.

The spectra of all of the benzenethiols were graphed together to determine whether or not there were any characteristic peaks that did not overlap, allowing for a ratiometric study to be performed. It was determined that there were 5 possible benzenethiol combinations that could be used in a ratiometric study. The pairings can be found in Figure 11 above.

The ratiometric study with benzenethiols was performed to determine the feasibility of quantitatively determining changing ratios in a mixture with SERS. It was possible to see characteristic peaks grow into the SERS spectra (Figure 19) however, there was not enough structural differentiation between the benzenethiol structures for

there to be fully independent characteristic peak sets. This would have allowed for the observation of a peak growing into the spectra while a different peak went away.

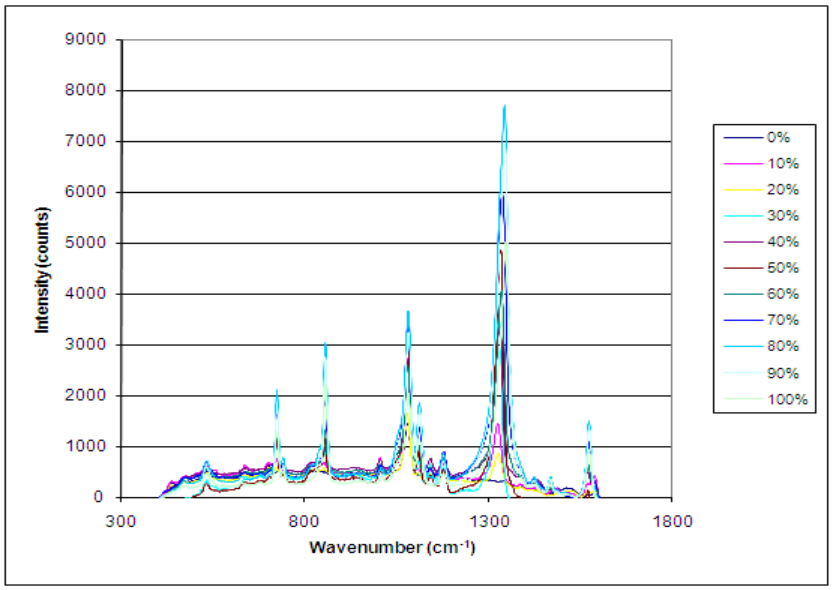

Figure 19: **Ratiometric Study between Benzenethiols.** 4-Nitrobenzenethiol and 4-Aminothiophenol solutions were ratioed volumetrically to track spectral changes.

Figure 20 shows a graph of the ratio of peak height to the area of the common peak at 1570 cm^{-1} as a function of 4-nitrobenzenethiol concentration in solution. The peaks at 724 and 1336 cm^{-1}, which can be attributed to the 4-nitrobenzenethiol, increase in relation to the area of the common peak as the concentration increases. There are strong correlation values for those trend lines meaning that there is a strong correlation between the peak intensity ratio and the percentage of 4-nitrobenzenethiol in the solution. The ratio for the peak at 1080 cm^{-1} decreases as the 4-aminothiophenol concentration decreases. This is consistent with what was expected as the peak at 1080 cm^{-1} can be attributed to the 4-aminothiophenol. The correlation value for this trendline is not as high, but the data for a pure solution of 4-aminothiophenol as well as a 20% solution are higher than the other data would suggest it should be.

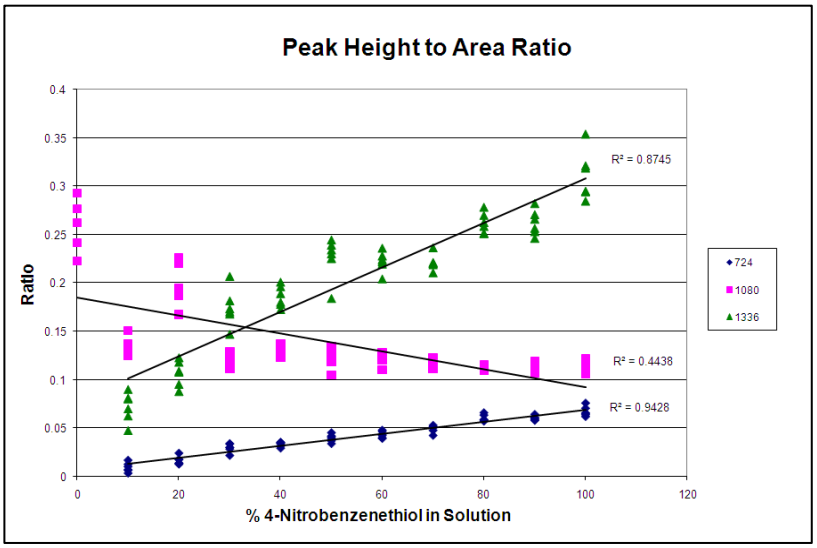

Figure 20: **Comparison of Selected Peak Heights to the Area of a Common Peak.** The peak intensities at 724, 1080 and 1336 cm^{-1} were ratioed to the area of the peak at 1570 cm^{-1} which was common to both benzenethiol spectra.

DNA Characterization

Spectra of the individual DNA bases were acquired to determine the characteristic peaks associated with each. The spectra can be found in Figure 21 below. The guanine chain was unstable when more than 3 residues were linked in succession. An adenine was inserted every fourth residue to stabilize the chain. This can be seen in the guanine spectra in Figure 21 as there is some peak overlap between the adenine and guanine spectra. The spectra acquired on AuNR substrates were compared to those acquired on AgNR substrates to see the DNA enhancement difference between the two substrate types. The spectra acquired on the AuNRs show the characteristic peaks for each of the DNA bases, however, the intensity of the signal is approximately an order of magnitude less than the intensity of peaks acquired on the AgNRs.

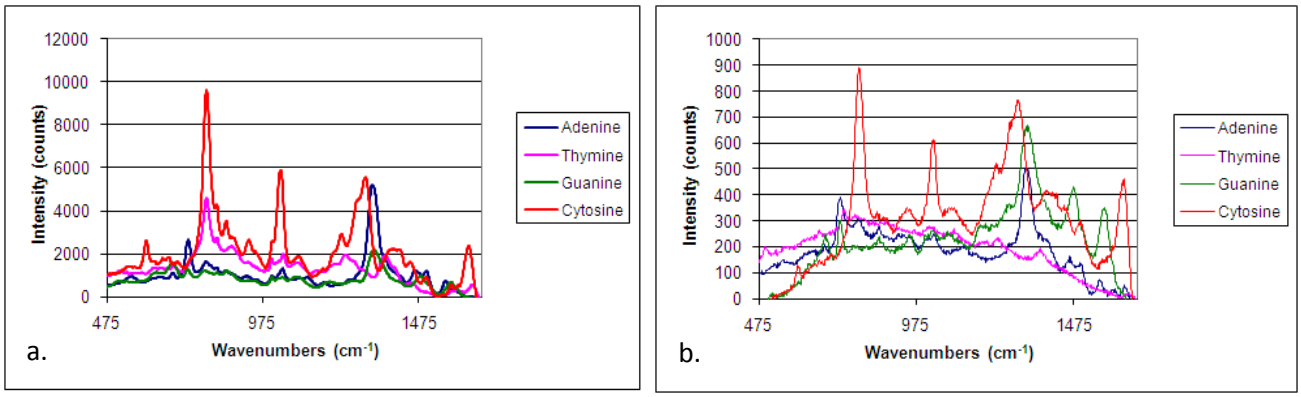

Figure 21: **SERS Spectra of DNA Bases on Silver (a) and Gold (b)**.

The spectra were analyzed and characteristic peak assignments were made for each of the DNA bases. The peak assignments can be found in Figure 22. The guanine response is generally lower in intensity than that of the other bases.

Figure 22: **Spectral Assignments of DNA Bases.**

Base	Assigned Wavenumbers
Adenine	728, 774, 1026, 1318
Cytosine	790, 1024, 1291, 1627
Guanine	680, 945, 1468, 1565
Thymine	771, 997, 1225, 1359

The spectra of the individual RSV oligos were obtained to confirm experimental results with the theoretical results. Figures 23 and 24 show characteristic SERS spectra of some of the RSV oligos. All of the individual ssDNA spectra can be found in Appendix B.

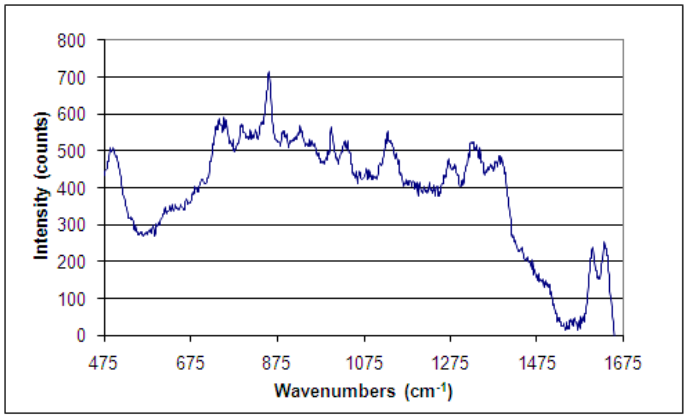

Figure 23: **SERS Spectrum of RSV 4**. The spectrum has been baseline subtracted.

As can be seen in Figure 23, the spectrum of RSV 4 has peaks characteristic of both adenine (733 cm^{-1}, 1036 cm^{-1} and 1311 cm^{-1}) and thymine (997 cm^{-1}, 1260 cm^{-1} and 1368 cm^{-1}). These peaks can be compared with the characteristic peaks listed in Figure 22. Of the 22 residues in the RSV 4 oligo, 11 are adenine and 5 are thymine. There are also 4 guanine residues and 2 cytosine residues. The recorded spectrum is consistent with what would be expected based on the sequence of RSV 4 (Figure 4.)

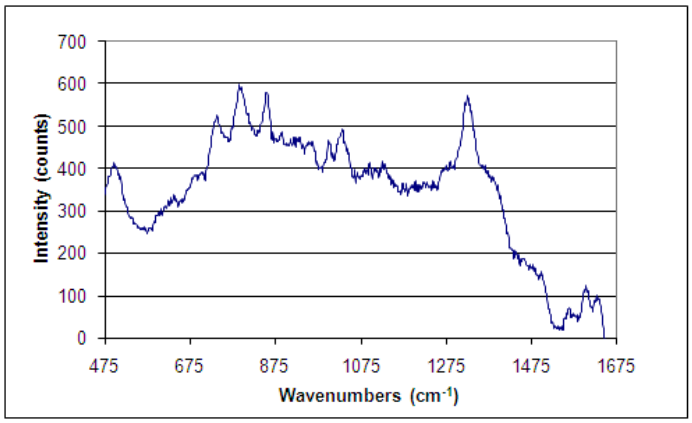

Figure 24: **SERS Spectrum of RSV 8**. The spectrum has been baseline subtracted.

Figure 24 shows peaks consistent with both adenine (726 cm^{-1} and 1323 cm^{-1}) and cytosine (787 cm^{-1} and 1018 cm^{-1}). These four peaks can be compared with the

characteristic peaks found in Figure 22. Over two thirds of the RSV 8 oligo sequence are comprised of adenine and cytosine residues. The spectrum found in Figure 24 is consistent with a DNA strand with that composition.

As mentioned earlier, buffer solutions interfered with the SERS signal and all further solutions were made in water. As DNA hybridization requires the presence of a salt, no actual hybridization was achieved. Equivolume aliquots of the DNA pairs being analyzed were mixed and the spectra taken. Figures 25 and 26 show the spectra of the DNA mixtures along with the spectra of the ssDNA components in the mixture. Both complimentary and non-complimentary DNA mixtures were examined spectroscopically. All of the mixture spectra from the study can be found in Appendix C.

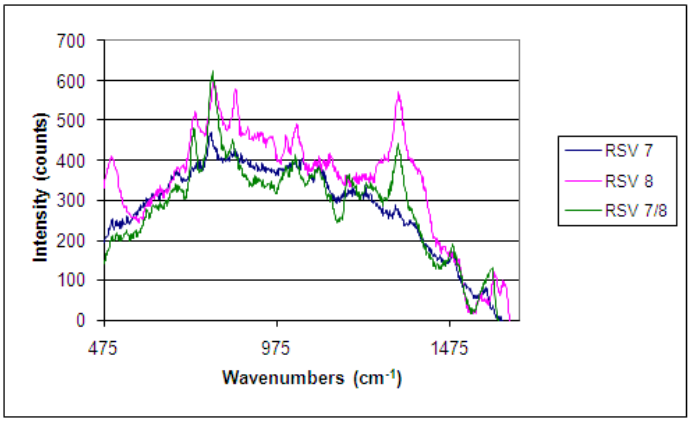

Figure 25: **Spectra of RSV 7, RSV 8 and the RSV 7 and RSV 8 Mixture**.

The spectrum of the RSV 7 and RSV 8 mixture shows peaks characteristic of both the RSV 7 and RSV 8 oligos. Visually, there is a greater contribution of the RSV 8 spectrum to that of the mixture. This can be attributed to the fact that the RSV 7 oligo was thiolated at the 5' end and the RSV 8 oligo was unthiolated. The thiol end group on the RSV 7 oligo bound to the AuNR surface which dictated the orientation of the ssDNA strand. SERS only detects the first 5-10 residues in the DNA strand. The 5' end of the

RSV 7 oligo begins with a sequence of TGGGGT which would have a very low intensity profile due to the low intensity of the guanine SERS response.

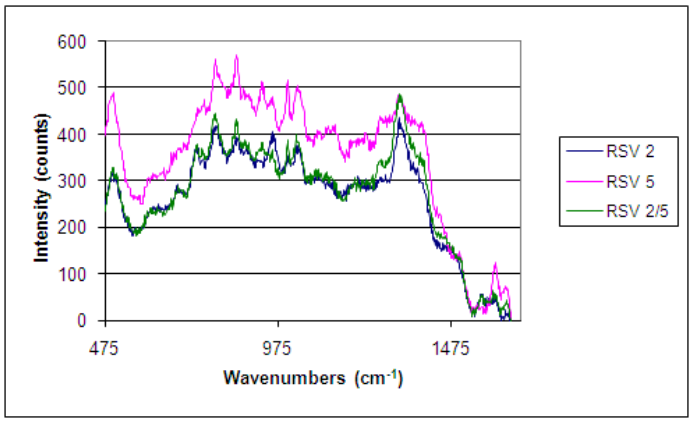

Figure 26: **Spectra of RSV 2, RSV 5 and the RSV 2 and RSV 5 Mixture.**

The sequences of RSV 2 and RSV 5 are the same for the first 5 residues beginning with the 5' end of each strand. The RSV 2 oligo was thiolated at the 5' end and thus bound to the AuNR substrate with that end. The RSV 5 oligo was not bound to the surface with any specificity of orientation, but it is apparent from the spectra that the 5' end of the RSV 5 was closest to the AuNR surface as well. As the enhancement is seen most strongly closest to the surface and decays exponentially with distance, it is understandable that the spectra of both RSV 2 and RSV 5 would be similar. It is possible to see a peak at ~843 cm^{-1} in the mixture spectrum appears only in the RSV 5 spectrum. It is also possible to see a peak at ~665 cm^{-1} in the mixture spectrum appears only in the RSV 2 spectrum. Even though the RSV 2 and RSV 5 sequences are very similar, it is still possible to distinguish between the two qualitatively and these differences are reflected in the mixture spectrum.

CHAPTER 4

CONCLUSIONS

Patterned AuNR arrays can be used as SERS substrates. The signal to noise ratio is lower on AuNR substrates than on the silver equivalent. A lower energy (higher wavelength) laser improves the intensity of the SERS signal from the AuNR substrate. Ozone cleaning the substrate prior to analyte deposition does not improve the signal however increasing the analyte volume does improve the signal strength. The analyte evaporates evenly across the surface of the well making location of spectral acquisition irrelevant.

Ratiometric changes of analyte concentrations can be tracked via SERS. It is necessary to have characteristic peaks that are unique to each of the analytes of interest for this to truly be of use. This allows for the possibility of quantification with the use of internal standards.

It is possible to detect characteristic nucleotide signals with AuNR SERS substrates. Spectra of DNA can then be compared with the characteristic nucleotide signals to qualitatively analyze the residues present in the sample. However, the poor signal to noise ratio makes it difficult to differentiate peaks from the background noise. Taking multiple spectra in each well and averaging the data helps with the noise issue but does not completely ameliorate the problem. The spectra obtained from SERS of DNA solution mixtures are simply a combination of the spectra from the ssDNA components.

Due to the weakness in SERS response and the low signal to noise ratio, AuNR substrates, while a viable option, are not the best choice for viral sensing with SERS. It is

also only possible to do qualitative analysis of the spectrum. This method is not practical unless the residue sequence being analyzed is known in advance for comparison. Even with the problems of surface oxidation quenching the SERS response, AgNR arrays are the better alternative at this point in time.

REFERENCES

Albrecht, M. G.; Creighton, J. A. Anomalously Intense Raman Spectra of Pyridine at a Silver Electrode. *J. Am. Chem. Soc*. [Online] **1977**, *99*(**15**), 5215-5217.

Arunkumar, K. A.; Bradley, E. B. Theory of Surface Enhanced Raman Scattering. *J. Chem. Phys*. **1983**, *78*(**6**), 2882-2888.

Bell, S. E. J.; Sirimuthu, N. M. S. Surface-Enhanced Raman Spectroscopy (SERS) for Sub-Microcolar Detection of DNA/RNA Mononucleotides. *J. Am. Chem. Soc*. [Online] **2006**, *128*, 15580-15581.

Caram, L. B.; Chen, J.; Taggart, E. W.; Hillyard, D. R.; She, R.; Polage, C. R.; Twersky, J.; Schmader, K.; Petti, C. A.; Woods, C. W. Respiratory Syncytial Virus Outbreak in a Long-Term Care Facility Detected Using Reverse Transcriptase Polymerase Chain Reaction: An Argument for Real-Time Detection Methods. *Journal of the American Geriatrics Society* [Online] **2009**, *57*, 482-485.

Centers for Disease Control and Prevention: Respiratory and Enteric Viruses Branch. Respiratory Syncytial Virus Webpage. http://www.cdc.gov/ncidod/dvrd/revb/respiratory/rsvfeat.htm (accessed May 22, 2007).

Chaney, S.; Shanmukh, S.; Dluhy, R.; Zhao, Y-P. Aligned Silver Nanorod Arrays Produce High Sensitivity Surface-Enhanced Raman Spectroscopy Substrates. *App. Phys. Lett*. [Online] **2005**, *87*, 031908.

Chávez-Bueno, S.; Mejías, A.; Jafri, H.; Ramilo, O. Respiratory Syncytial Virus: Old Challenges and New Approaches. Pediatric Annals [Online] **2005**, *34*(**1**), 62-68.

Department of Metallurgy, Electrochemistry and Materials Science. Raman Spectroscopy Webpage. http://www.vub.ac.be/META/toestellen_raman.php?m=xpand&d=menu7 (accessed April 12, 2009).

Driskell, J.; Shanmukh, S.; Liu, Y.; Hennigan, S.; Jones, L.; Zhao, Y-P; Dluhy, R.A.; Krause, D.C.; Tripp, R.A. Infectious Agent Detection with SERS-Active Silver Nanorod Arrays Prepared by Oblique Angle Deposition. *IEEE Sens. J*. [Online] **2008**, *8*(**6**), 863-870.

Driskell, J.; Shanmukh, S.; Liu, Y.; Chaney, S.; Tang, X-J; Zhao, Y-P; Dluhy, R. The Use of Aligned Silver Nanorod Arrays Prepared by Oblique Angle Deposition as Surface Enhanced Raman Scattering Substrates. *J. Phys. Chem. C* [Online] **2008**, *12*(**4**), 895-901.

Fang, C.; Agarwal, A.; Buddharaju, K.D.; Khalid, N.M.; Salim, S.M.; Widjaja, E.; Garland, M.V.; Balasubramanian, N.; Kwong, D.L.. DNA Detection Using Nanostructured SERS substrates with Rhodamine B as Raman Label. *Biosens. Bioelectron*. [Online] **2008**, *24*, 216-221.

Fleischmann, M.; Hendra, P.J.; McQuillan, A. J. Raman Spectroscopy of Pyridine Adsorbed at a Silver Electrode. *Chem. Phys. Lett.* **1974**, *26*(**2**), 163-166.

Fourier Transform Raman Spectroscopy: From Concept to Experiment; Chase, D. B.; Rabolt, J. F., Eds.; Academic Press: San Diego, CA, 1994.

Gersten, J.; Nitzan, A. Electromagnetic Theory of Enhanced Raman Scattering by Molecules Adsorbed on Rough Surfaces. *J. Chem. Phys*. **1980**, *73*(**7**), 3023-3037.

Gish, D. A.; Nsiah, F.; McDermott, M. T.; Brett, M. J. Localized Surface Plasmon Resonance Biosensor using Silver Nanostructures Fabricated by Glancing Angle Deposition. *Anal. Chem*. [Online] **2007**, *79*, 4228-4232.

Green, M.; Liu, F.M.; Cohen, L.; Köllensperger, P.; Cass, T.. SERS Platforms for High Density DNA Arrays. *Faraday Discuss*. [Online] **2006**, *132*, 269-280.

Jans, K.; Bonroy, K.; DePalma, R.; Reekmans, G.; Jans, H.; Laureyn, W.; Smet, M.; Borghs, G.; Maes, G. Stability of Mixed PEO-Thiol SAMs for Biosensing Applications. *Langmuir* [Online] **2008**, *24*, 3949-3954.

Jeanmaire, D. L.; Van Duyne, R. P. Surface Raman Spectroelectrochemistry: Part I. Heterocyclic, Aromatic, and Aliphatic Amines Adsorbed on the Anodized Silver Electrode. *J. Electroanal. Chem*. [Online] **1977**, *84*, 1-20.

Kim, K.; Lee, I.; Lee, S.J.. Photolytics Reduction of 4-Nitrobenzenethiol on Au Mediated via Ag Nanoparticles. *Chem. Phys. Lett.* [Online] **2003**, *377*, 201-204.

King, F. W.; Van Duyne, R. P.; Schatz, G. C. Theory of Raman Scattering by Molecules Adsorbed on Electrode Surfaces. *J. Chem. Phys*. **1978**, *69*(**10**), 4472-4481.

Kudelski, A.. Structures of Monolayers Formed from Different HS-(CH2)2-X Thiols on Gold, Silver and Copper: Comparitive Studies by Surface-Enhanced Raman Scattering. *J. Raman Spectrosc*. [Online] **2003**, *34*, 853-862.

Maksymovych, P.; Yates, J. T. Jr. Au Adatoms in Self-Assembly of Benzenethiol on the Au(111) Surface. *J. Am. Chem. Soc*. [Online] **2008**, *130*(**24**), 7518-7519.

Marotta, N.; Barber, J.; Dluhy, P.; Bottomley, L. Patterned Nanoarray Substrates for Biosensing with Surface Enhanced Raman Scattering. (Manuscript in progress.)

Martínez, J. L.; Gao, Y,; López-Ríos, T. Surface-Enhanced Raman Scattering of Obliquely Evaporated Ag Films. *Phys. Rev. B* [Online] **1986**, *33*(**8**), 5917-5919.

Moskovits, M., Surface-Enhanced Spectroscopy. *Reviews of Modern Physics*, [Online] **1985**. *57*(**3**), 783-826.

McCall, S. L.; Platzman, P. M.; Wolff, P.A. Surface Enhanced Raman Scattering. *Phys. Lett. A*. **1980**, *77*(**5**), 381-383.

McCreery, Richard L. *Raman Spectroscopy for Chemical Analysis*; Winefordner, J. D., Ed.; Wiley Interscience: New York, **2000**.

Mulvaney, S. P.; Keating, C. D. Raman Spectroscopy. *Anal. Chem*. [Online] **2000**, *72*, 145R-157R.

Otto, C.; van den Tweel, T. J. J.; de Mul, F. F. M.; Greve, J.. Surface-Enhanced Raman Spectroscopy of DNA Bases. *J. Raman Spectrosc*. **1986**, *17*(**3**), 289-297.

Raman, C. V. A New Radiation. *Indian J. Phys*. **1928**, *2*, 387-398.

Raman, C. V.; Krishnan, K. S. A New Class of Spectra due to Secondary Radiation. I. *Indian J. Phys*. **1928**, *2*, 399-419.

Robbie, K.; Sit, J. C.; Brett, M. J. Advanced Techniques for Glancing Angle Deposition. *J. Vac. Sci. Technol. B* [Online] **1998**, *16*(**3**), 1115-1122.

Ru, E. C.; Blackie, E.; Meyer, M.; Etchegoin, P. G. Surface Enhanced Raman Scattering Enhancement Factors: A Comprehensive Study. *J. Phys. Chem. C* [Online] **2007**, *111*, 13794-13803.

Shanmukh, S.; Jones, L.; Zhao, Y-P.; Driskell, J. D.; Tripp, R. A.; Dluhy, R. A. Identification and Classification of Respiratory Syncytial Virus (RSV) Strains by Surface-Enhanced Raman Spectroscopy and Multivariate Statistical Techniques. *Anal. Bioanal. Chem*. [Online] **2008**, *390*, 1551-1555.

Shanmukh, S.; Jones, L.; Driskell, J.; Zhao, Y-P.; Dluhy, R.; Tripp, R. Rapid and Sensitive Detection of Respiratory Virus Molecular Signatures Using a Silver Nanorod Array SERS Substrate. *Nano Lett.* [Online] **2006**, *6*, 2630 – 2636.

Skoog, D. A.; Holler, F. J.; Crouch, S. R. Raman Spectroscopy. *Principles of Instrumental Analysis*; Thomson Brooks/Cole: Belmont, CA, 2007; pp 481 – 497.

Strobel, H. A. Raman Spectroscopy. *Chemical Instrumentation: A Systematic Approach*, 2nd ed.; Addison-Wesley Publishing Co.: Massachusetts, 1973.

Tansil, N.; Gao, Z. Nanoparticles in Biomolecular Detection. *Nano Today* [Online] **2006**, *1*(**1**), 28-37.

Thierry, B.; Ng, J.; Krieg, T.; Griesser, H J. A Robust Procedure for the Functionalization of Gold Nanorods and Noble Metal Particles. *Chem. Commun*. [Online] **2009**, *13*, 1724-1726.

Vo-Dinh, T.; Stokes, D. L.; Griffin, G. D.; Volkan, M.; Kim, U. J.; Simon, M. I. Surface-Enhanced Raman Scattering (SERS) Method and Instrumentation for Genomics and Biomedical Analysis. *J. Raman Spectrosc.* [Online] **1999**, *30*, 785-793.

Appendix A

All Spectra from the Ozone and Volume Study

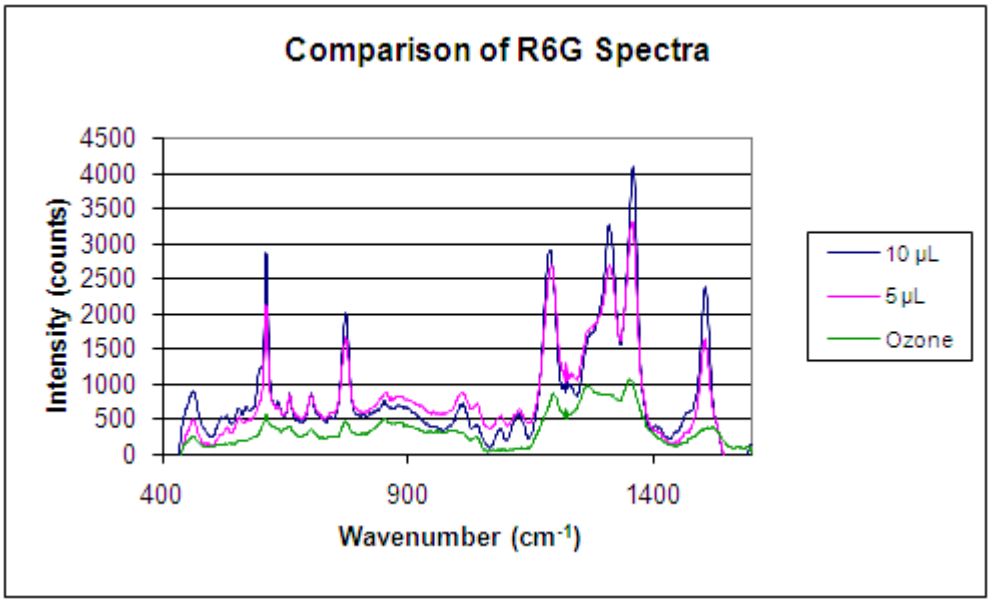

Figure A1: **Rhodamine 6G Spectra from Volume and Ozone Study.**

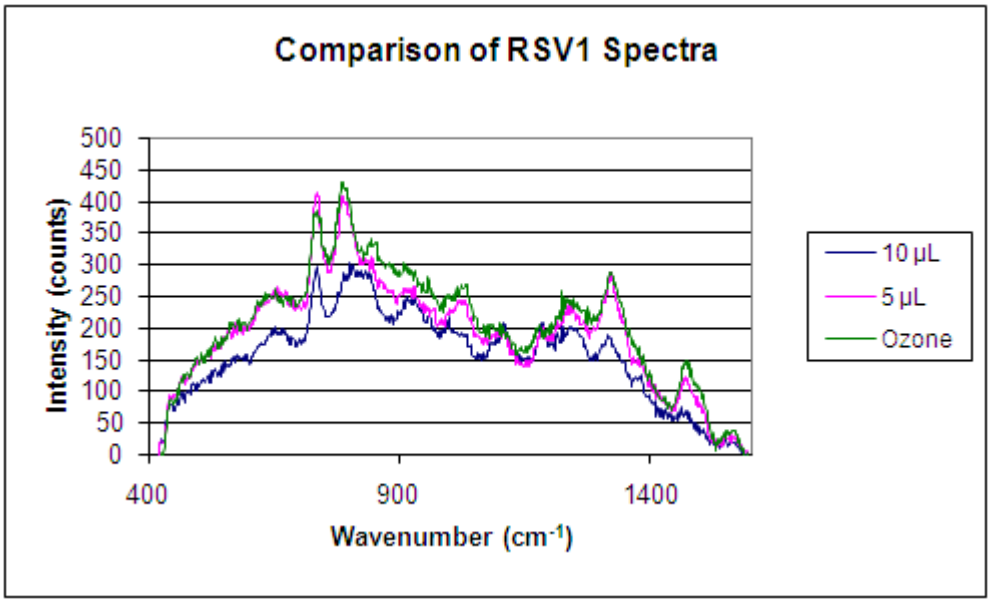

Figure A2: **RSV 1 Spectra from Volume and Ozone Study.**

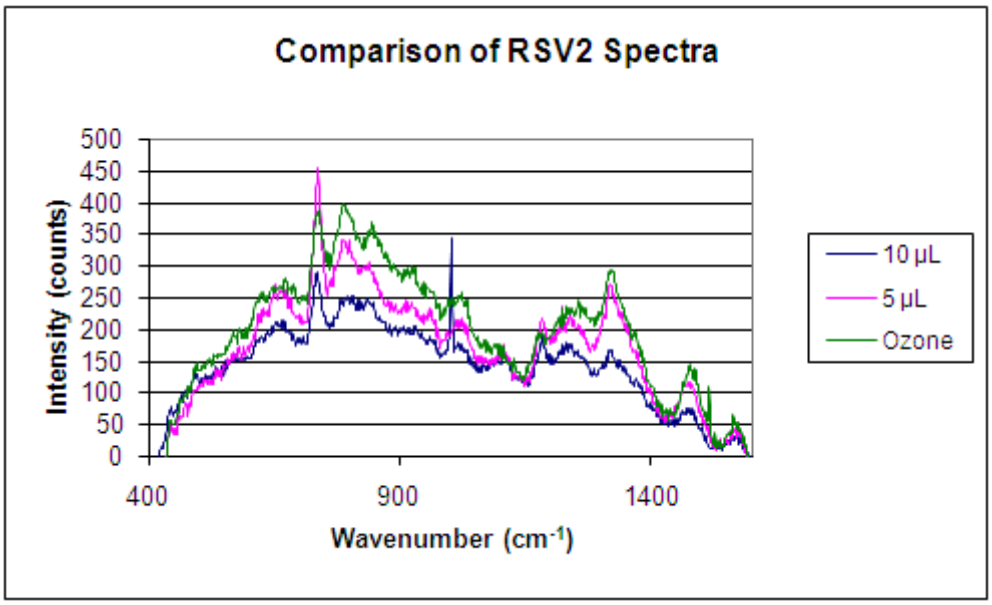

Figure A3: **RSV 2 Spectra from Volume and Ozone Study.**

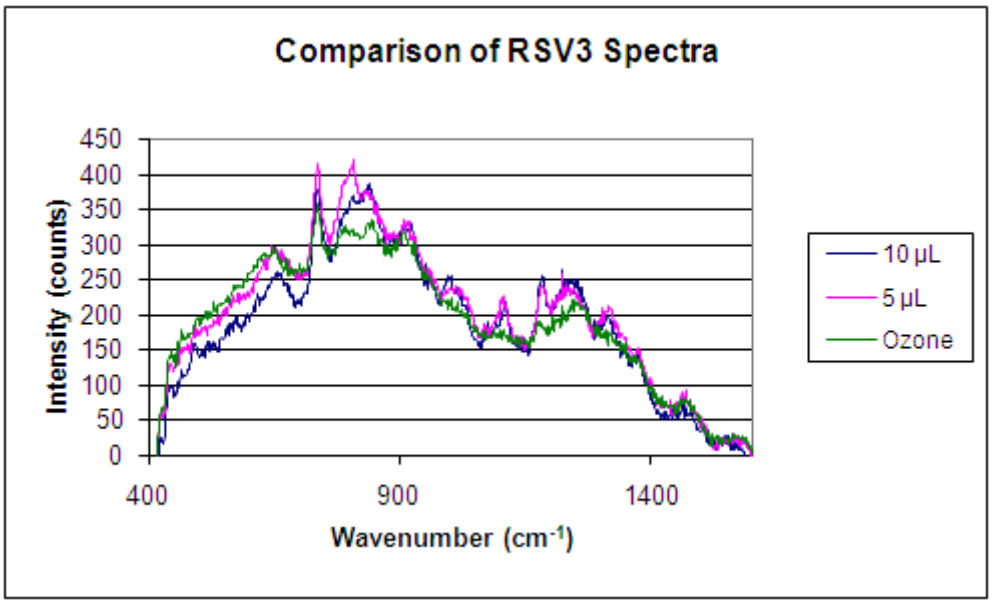

Figure A4: **RSV 3 Spectra from Volume and Ozone Study.**

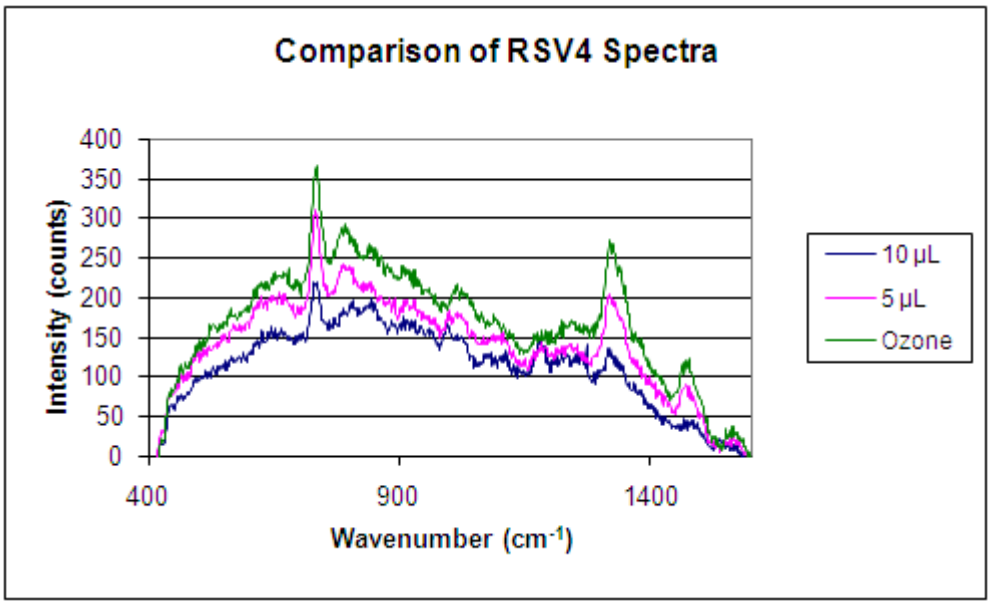

Figure A5: **RSV 4 Spectra from Volume and Ozone Study.**

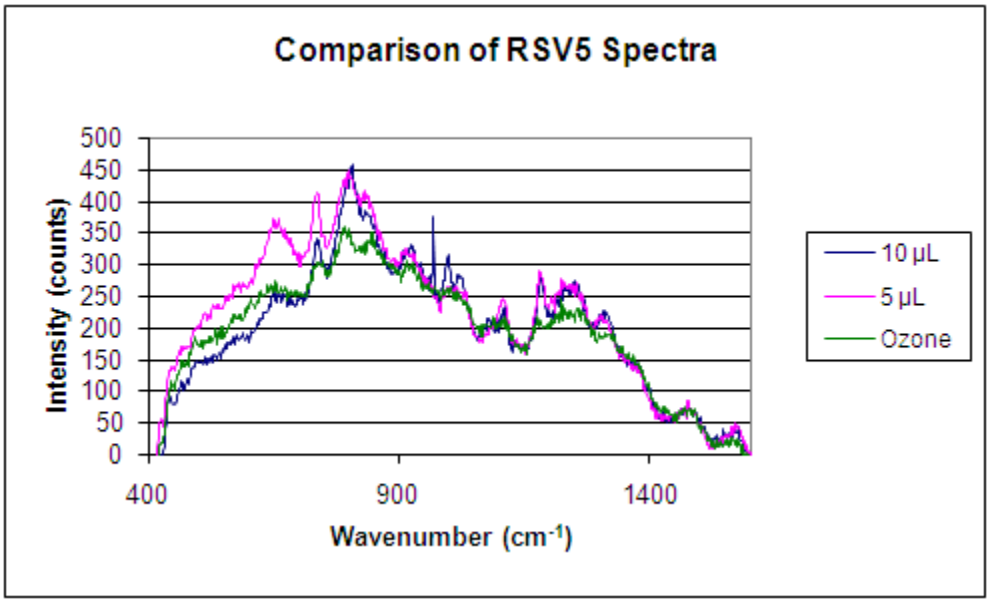

Figure A6: **RSV 5 Spectra from Volume and Ozone Study.**

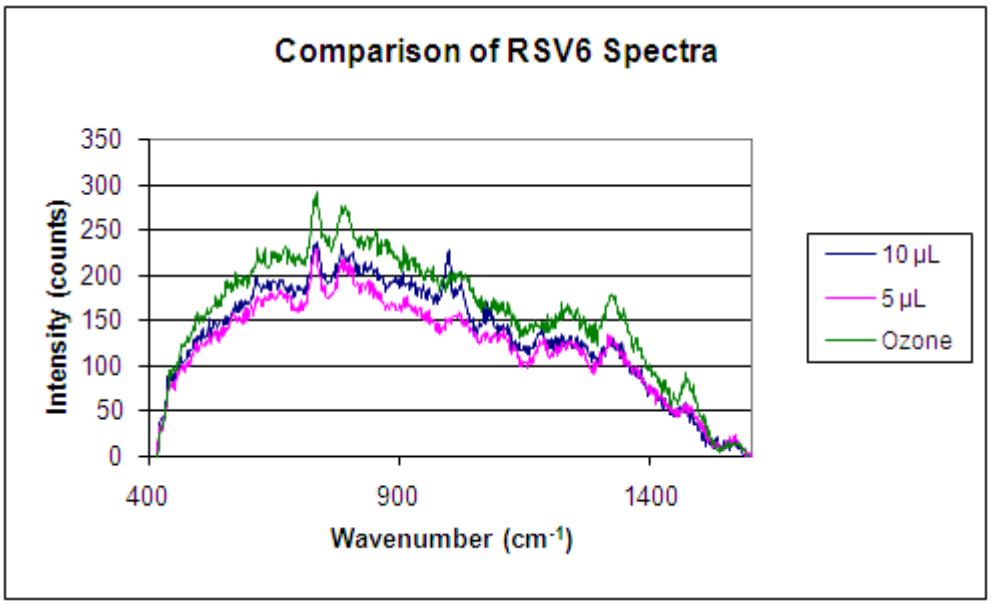

Figure A7: **RSV 6 Spectra from Volume and Ozone Study.**

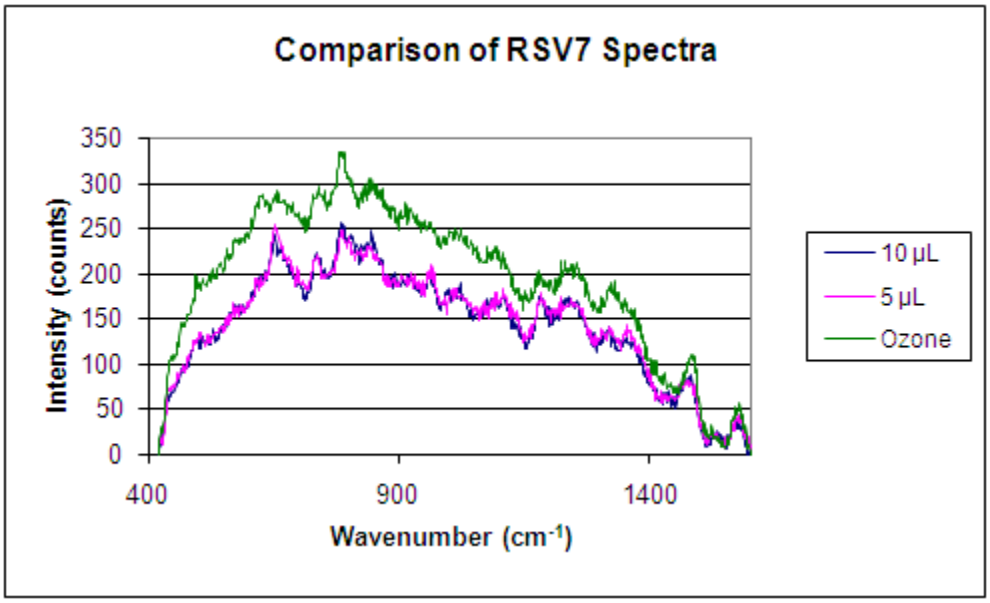

Figure A8: **RSV 7 Spectra from Volume and Ozone Study.**

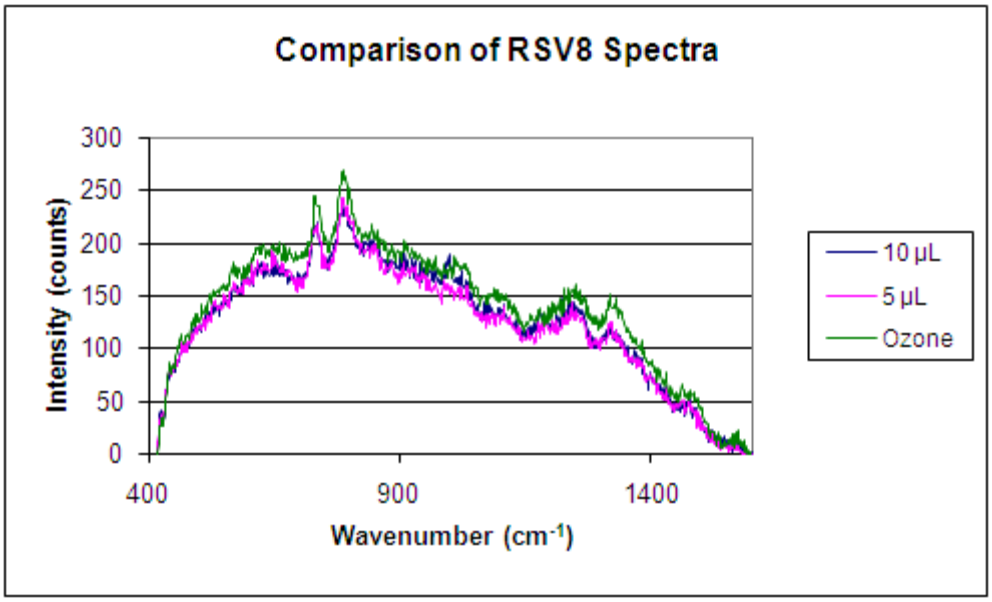

Figure A9: **RSV 8 Spectra from Volume and Ozone Study.**

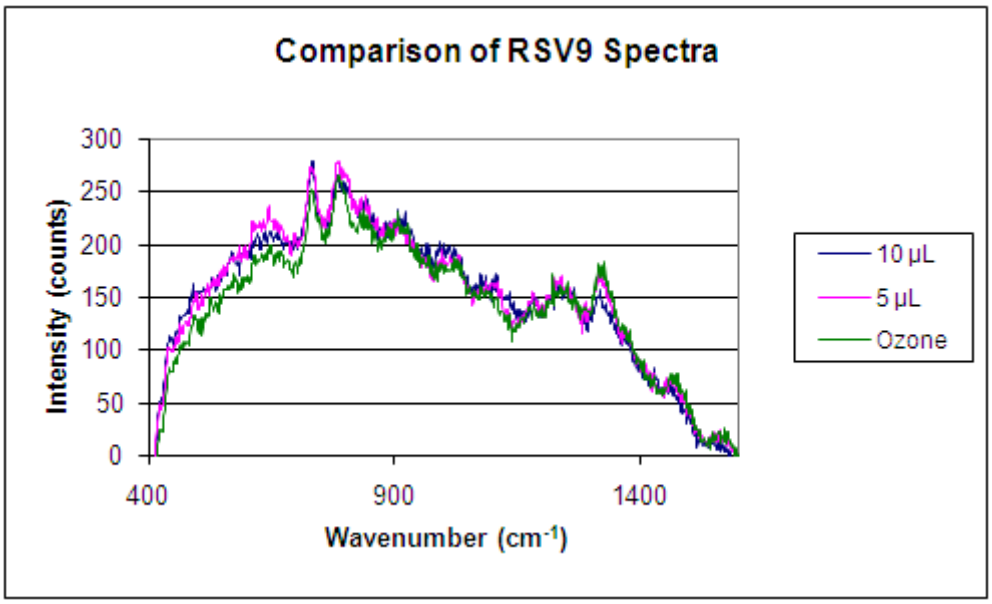

Figure A10: **RSV 9 Spectra from Volume and Ozone Study.**

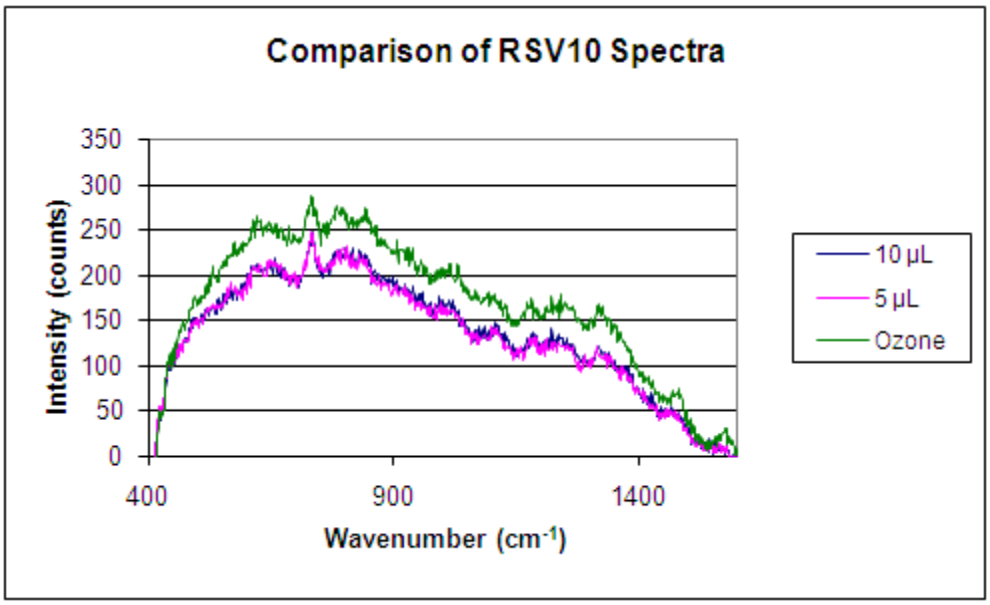

Figure A11: **RSV 10 Spectra from Volume and Ozone Study.**

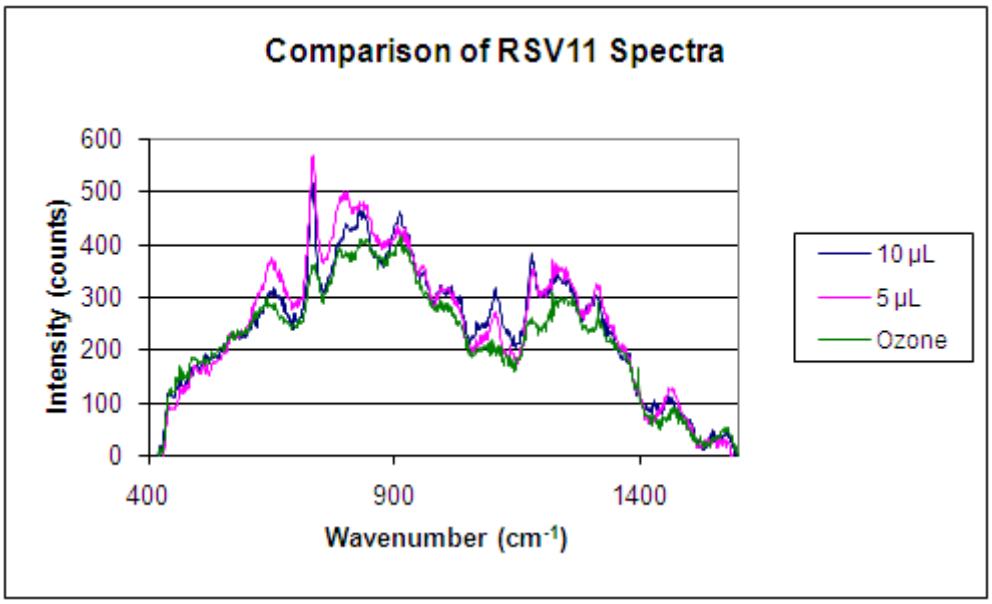

Figure A12: **RSV 11 Spectra from Volume and Ozone Study.**

Appendix B

All ssDNA Spectra

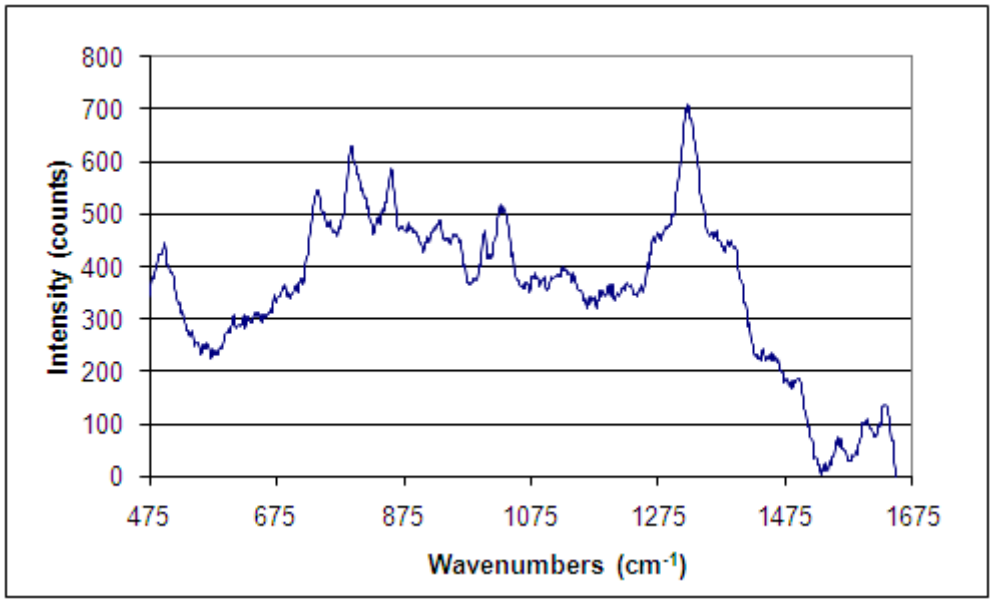

Figure B1: **RSV 1 Spectrum in Nanopure Water.**

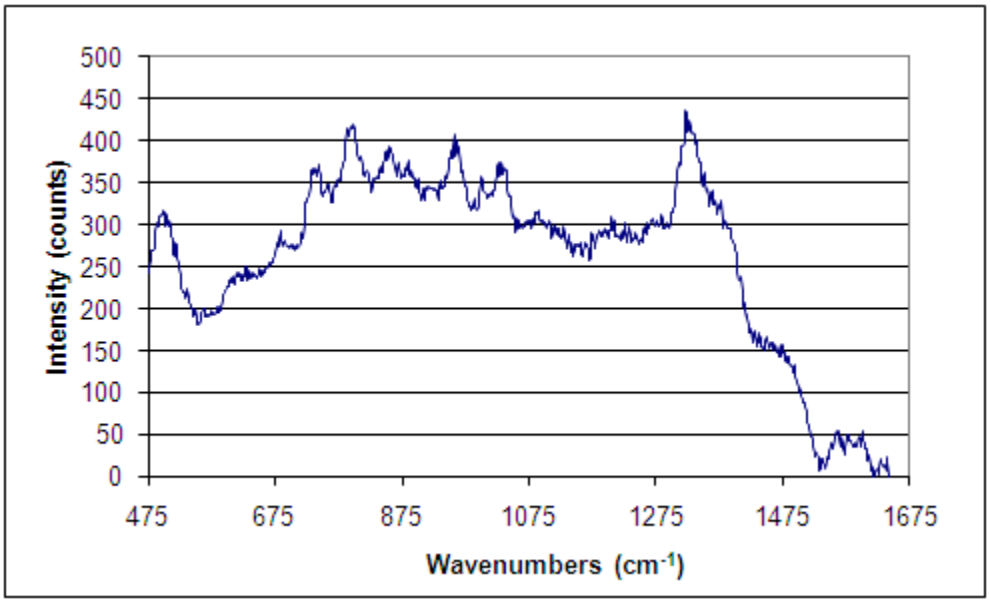

Figure B2: **RSV 2 Spectrum in Nanopure Water.**

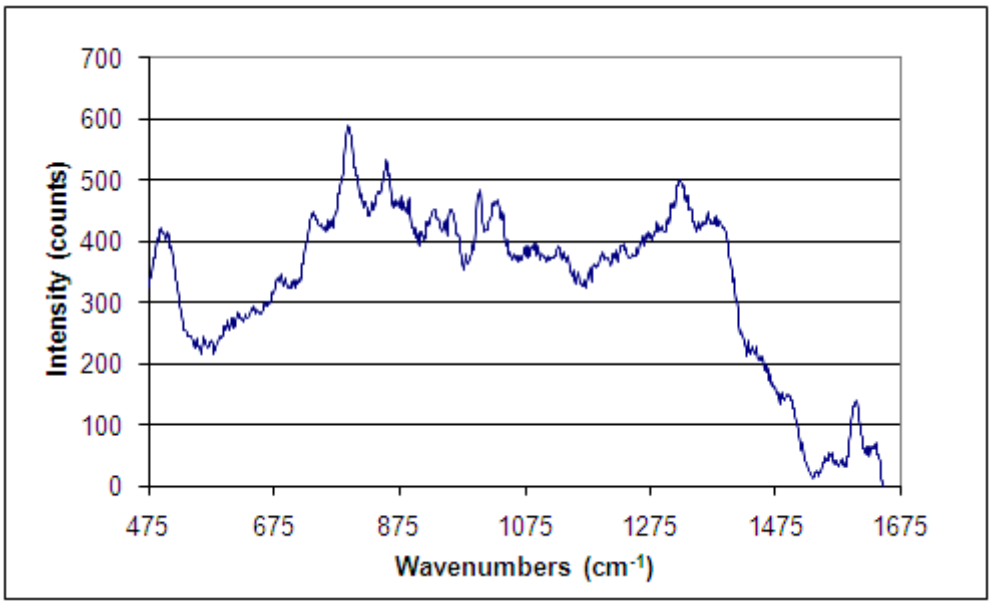

Figure B3: **RSV 3 Spectrum in Nanopure Water.**

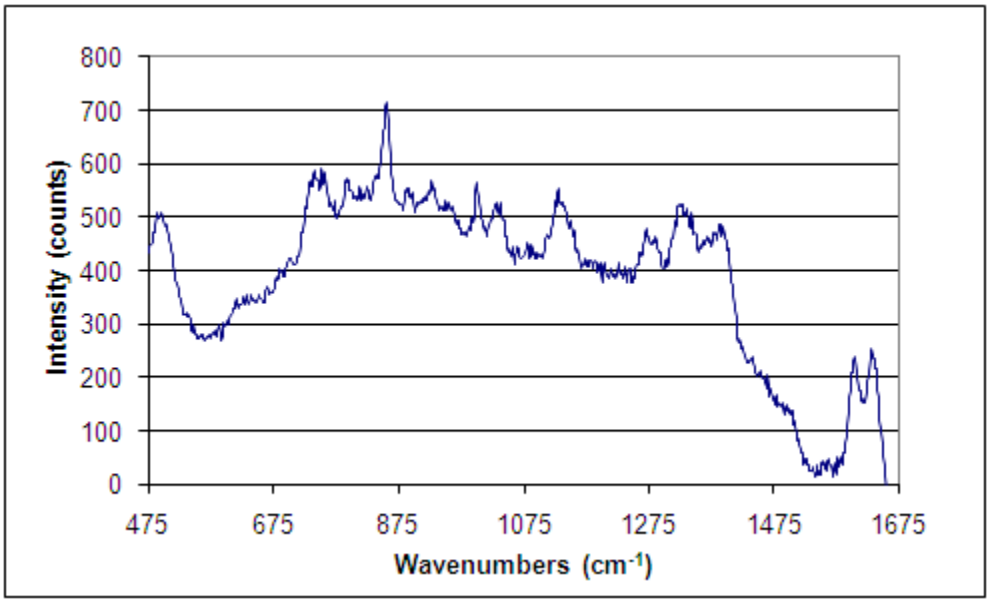

Figure B4: **RSV 4 Spectrum in Nanopure Water.**

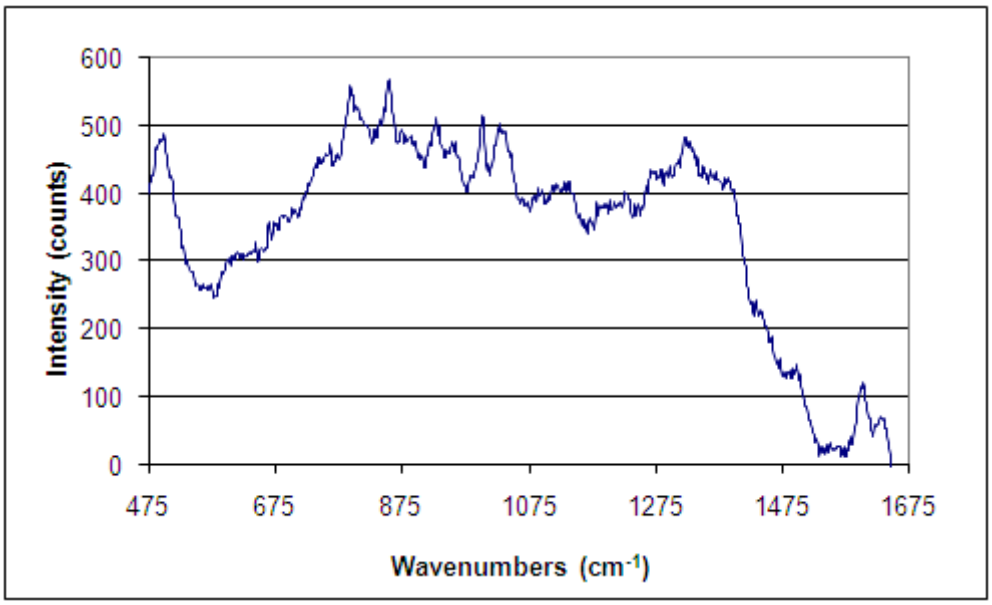

Figure B5: **RSV 5 Spectrum in Nanopure Water.**

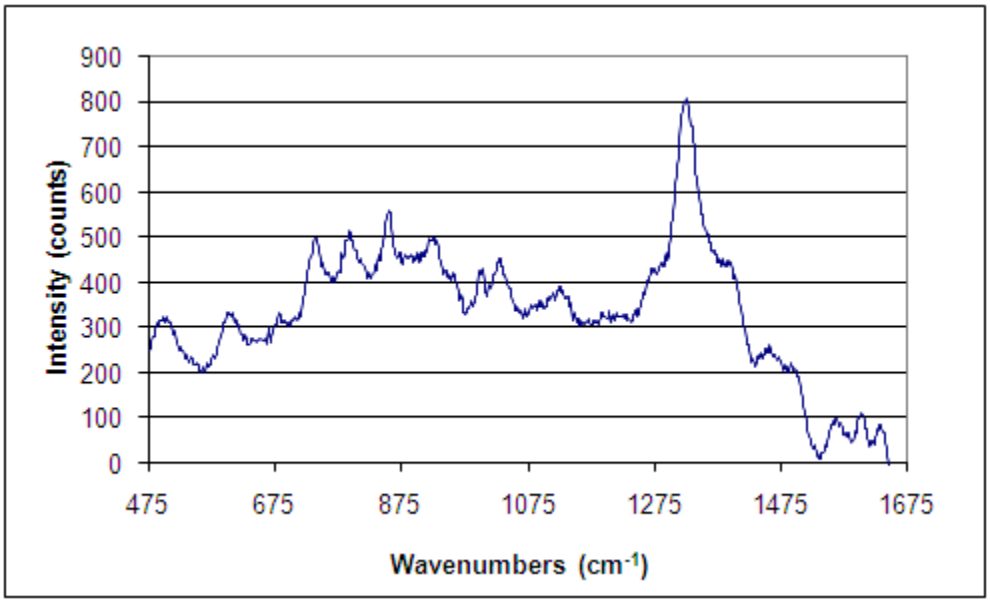

Figure B6: **RSV 6 Spectrum in Nanopure Water.**

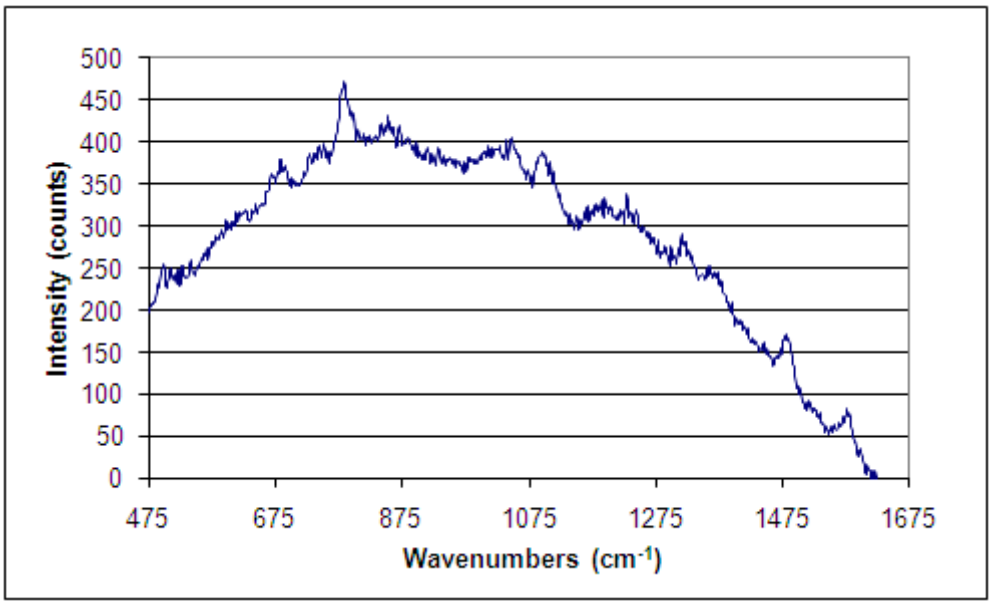

Figure B7: **RSV 7 Spectrum in Nanopure Water.**

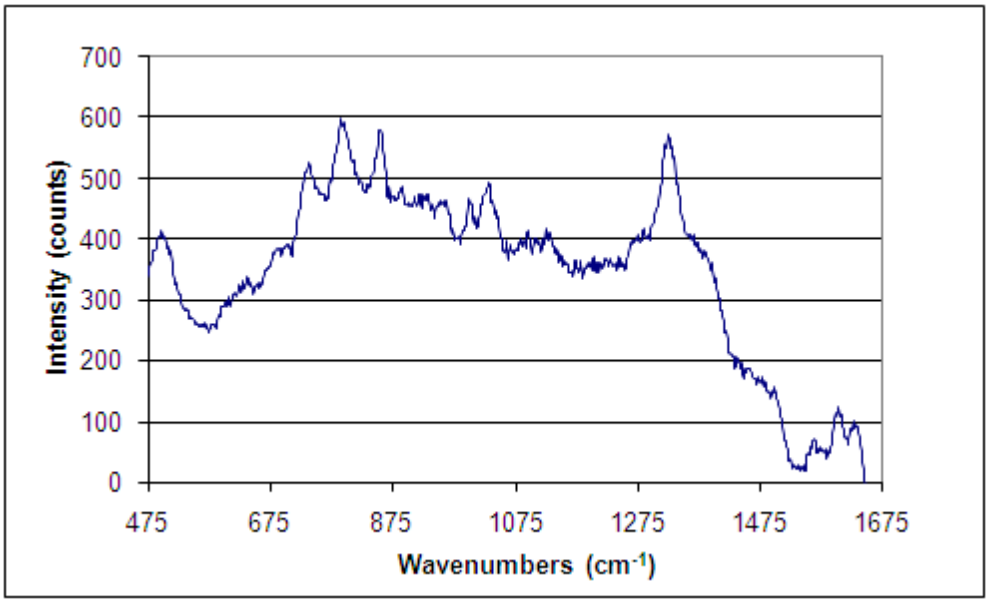

Figure B8: **RSV 8 Spectrum in Nanopure Water.**

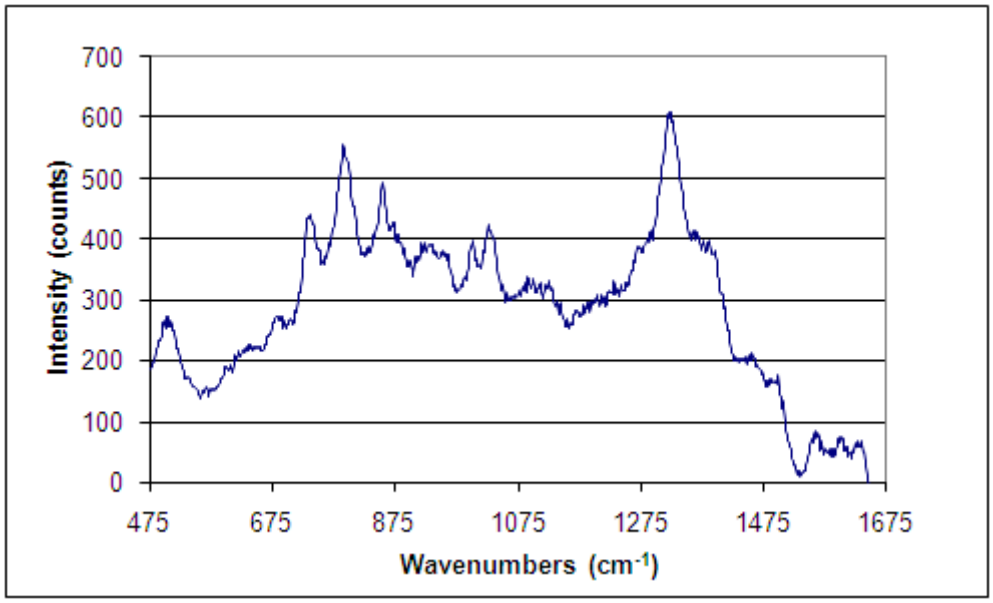

Figure B9: **RSV 9 Spectrum in Nanopure Water.**

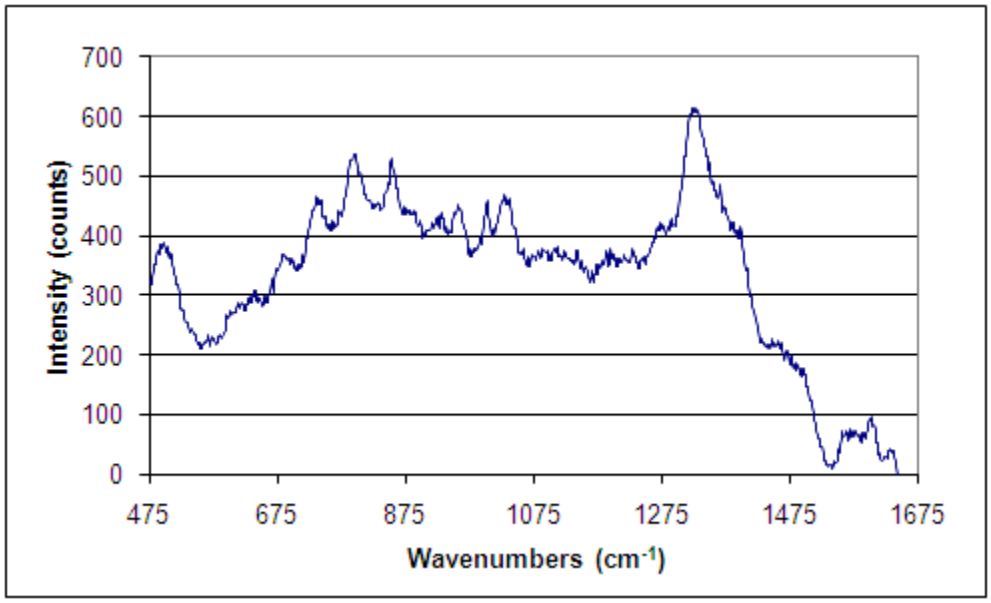

Figure B10: **RSV 10 Spectrum in Nanopure Water.**

Appendix C

All Spectra from the DNA mixtrue Study

Complimentary dsDNA

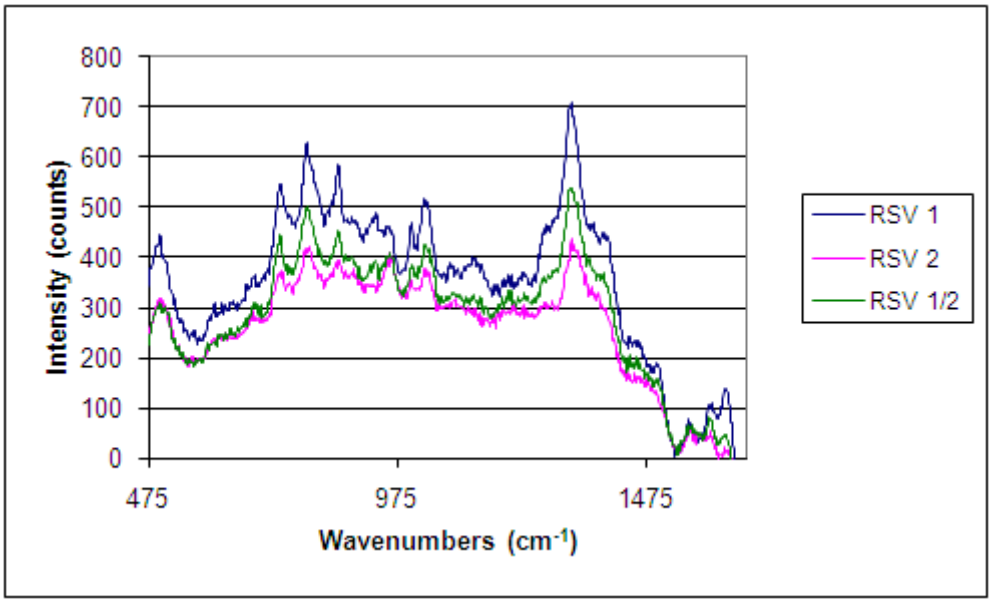

Figure C1: **Spectrum of RSV 1 and RSV 2 mixture with RSV 1 and RSV 2 Spectra in Nanopure Water.**

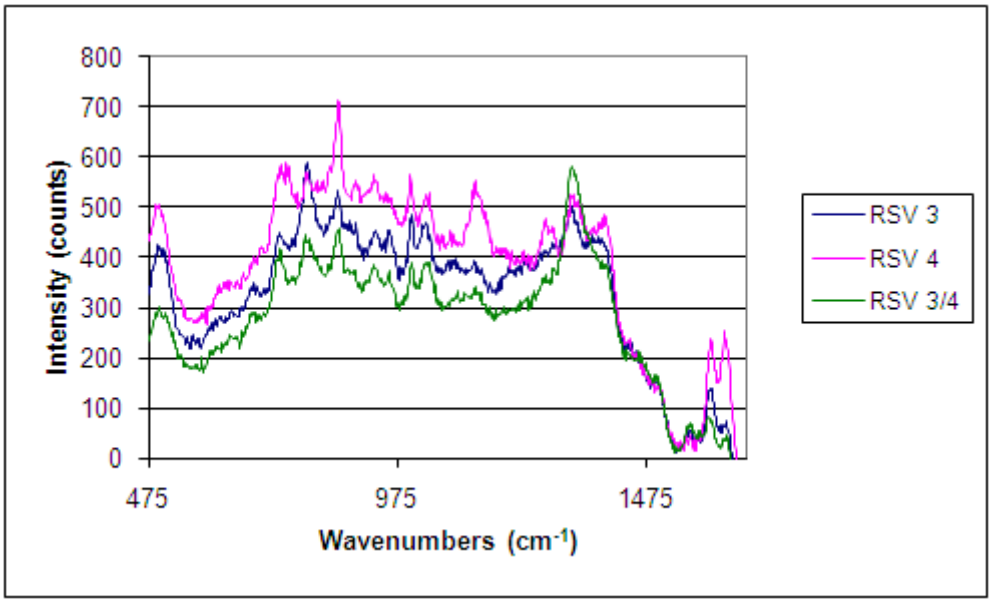

Figure C2: **Spectrum of RSV 3 and RSV 4 mixture with RSV 3 and RSV 4 Spectra in Nanopure Water.**

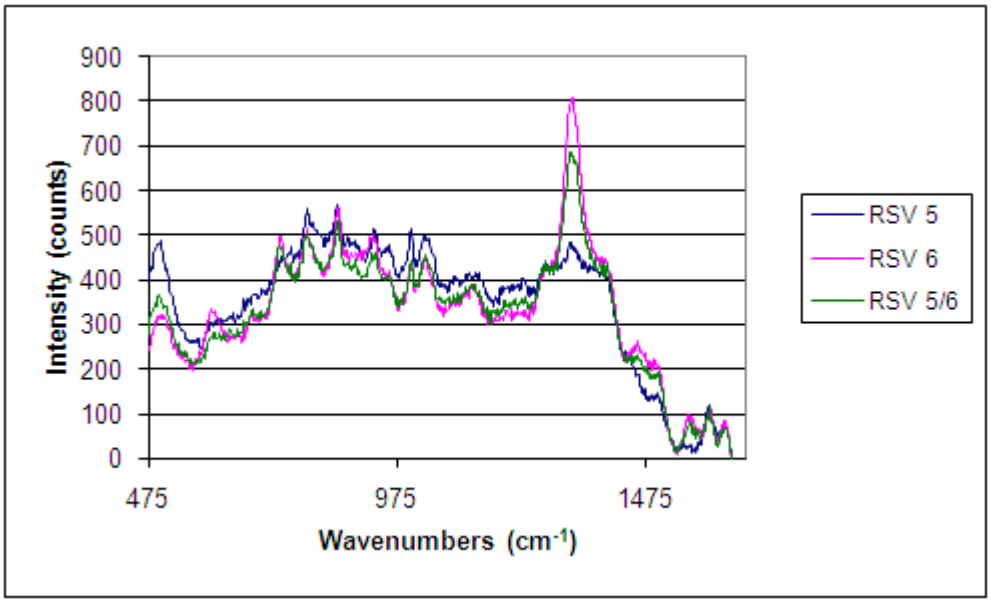

Figure C3: **Spectrum of RSV 5 and RSV 6 mixture with RSV 5 and RSV 6 Spectra in Nanopure Water.**

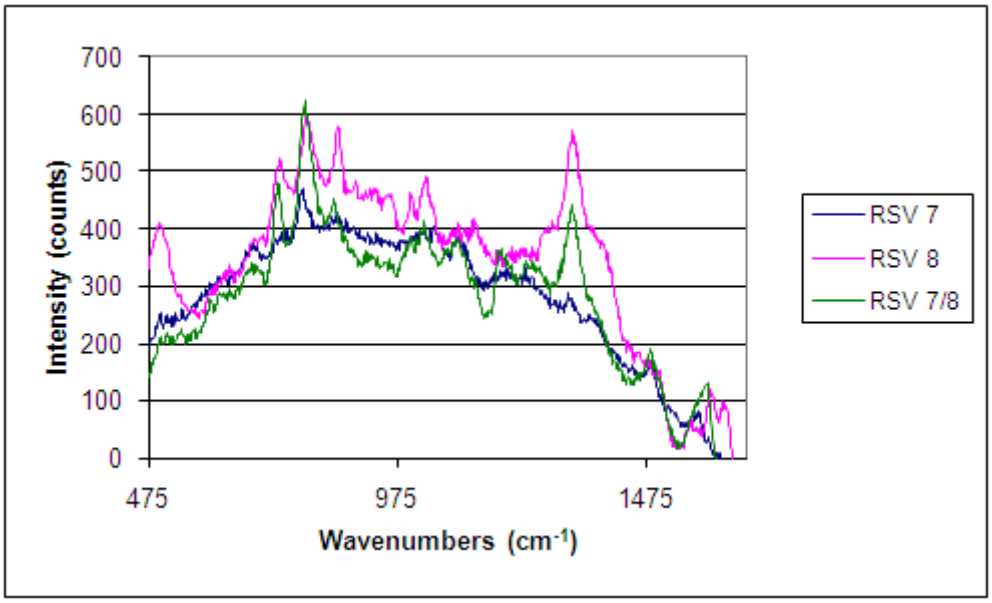

Figure C4: **Spectrum of RSV 7 and RSV 8 mixture with RSV 7 and RSV 8 Spectra in Nanopure Water.**

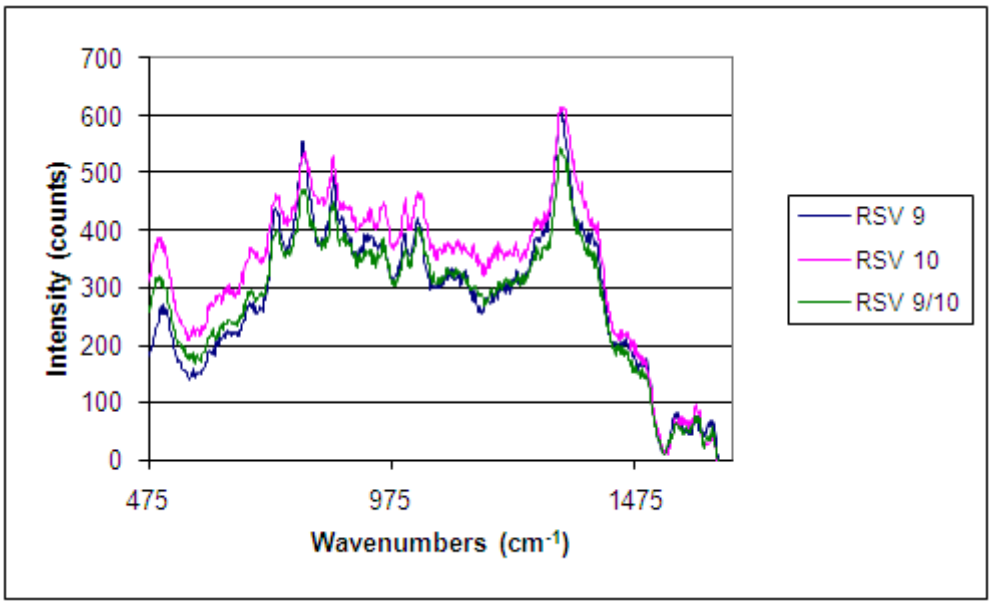

Figure C5: **Spectrum of RSV 9 and RSV 10 mixture with RSV 9 and RSV 10 Spectra in Nanopure Water.**

Non-Complimentary dsDNA

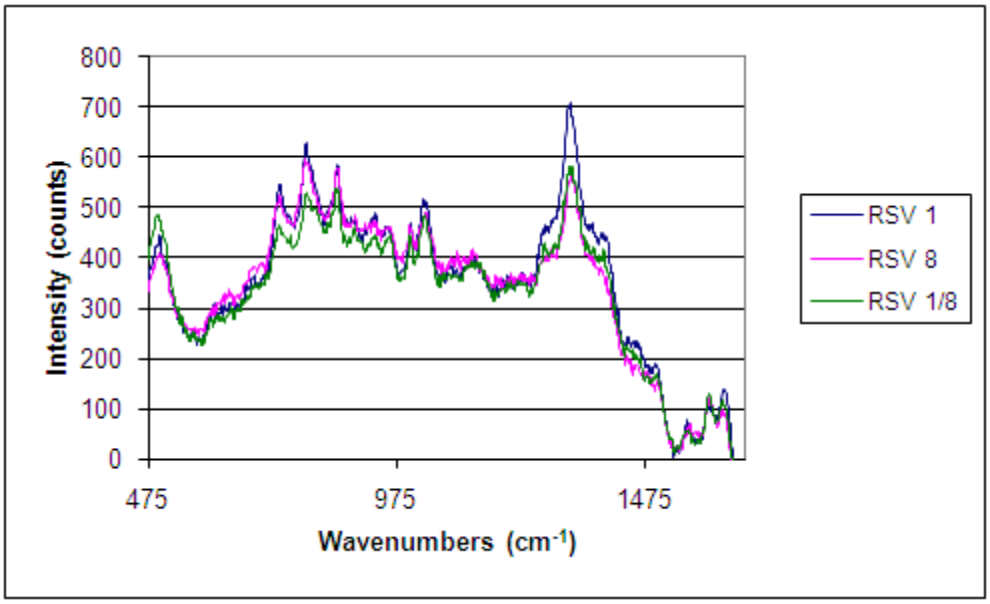

Figure C6: **Spectrum of RSV 1 and RSV 8 mixture with RSV 1 and RSV 8 Spectra in Nanopure Water.**

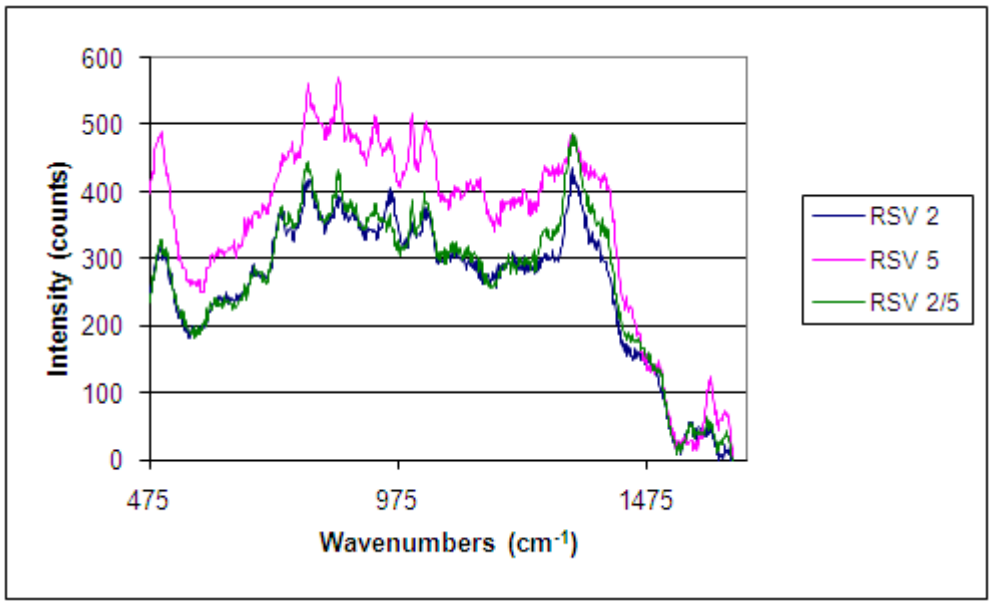

Figure C7: **Spectrum of RSV 2 and RSV 5 mixture with RSV 2 and RSV 5 Spectra in Nanopure Water.**

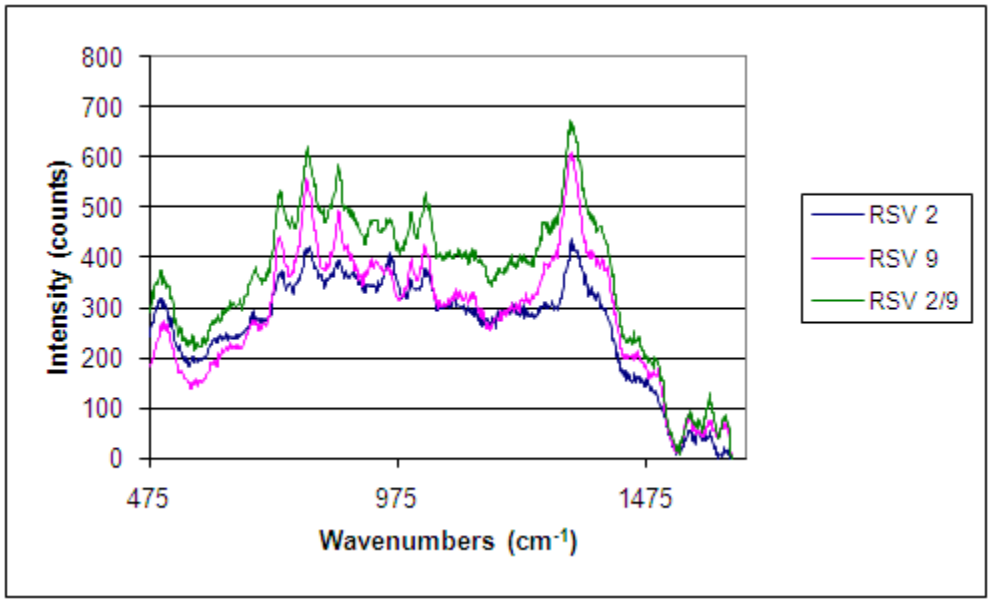

Figure C8: **Spectrum of RSV 2 and RSV 9 mixture with RSV 2 and RSV 9 Spectra in Nanopure Water.**

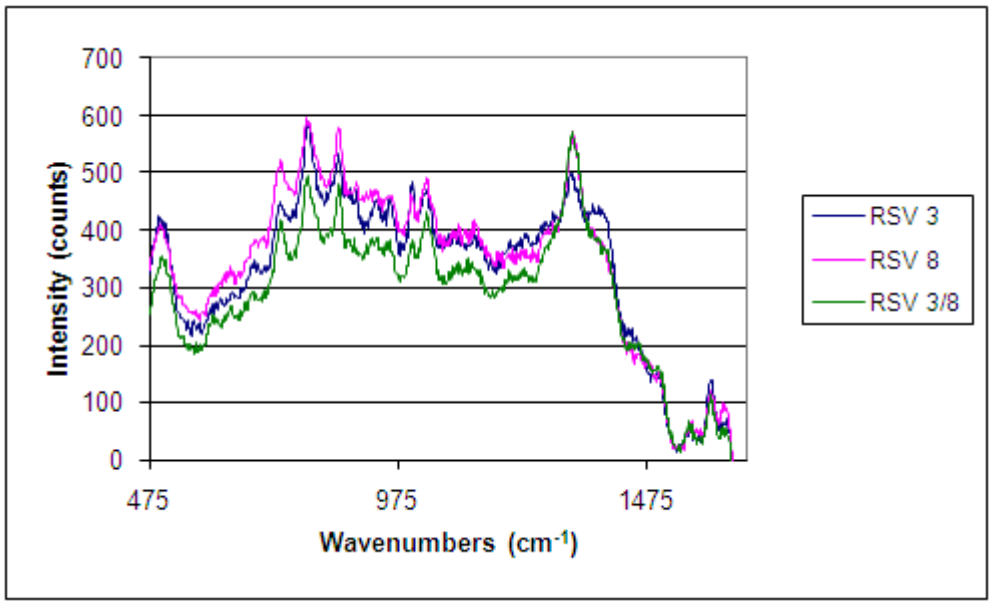

Figure C9: **Spectrum of RSV 3 and RSV 8 mixture with RSV 3 and RSV 8 Spectra in Nanopure Water.**

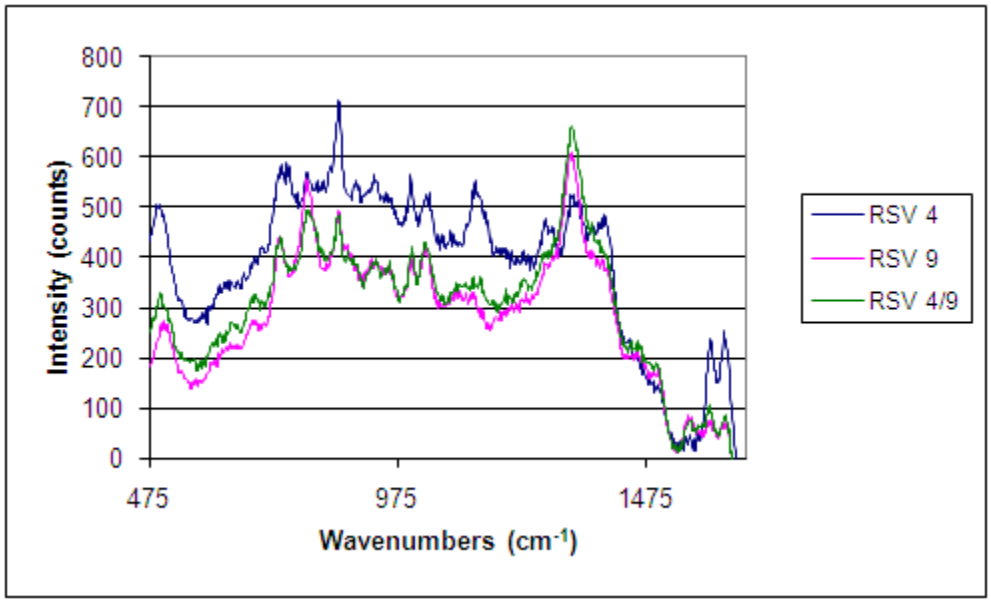

Figure C10: **Spectrum of RSV 4 and RSV 9 mixture with RSV 4 and RSV 9 Spectra in Nanopure Water.**

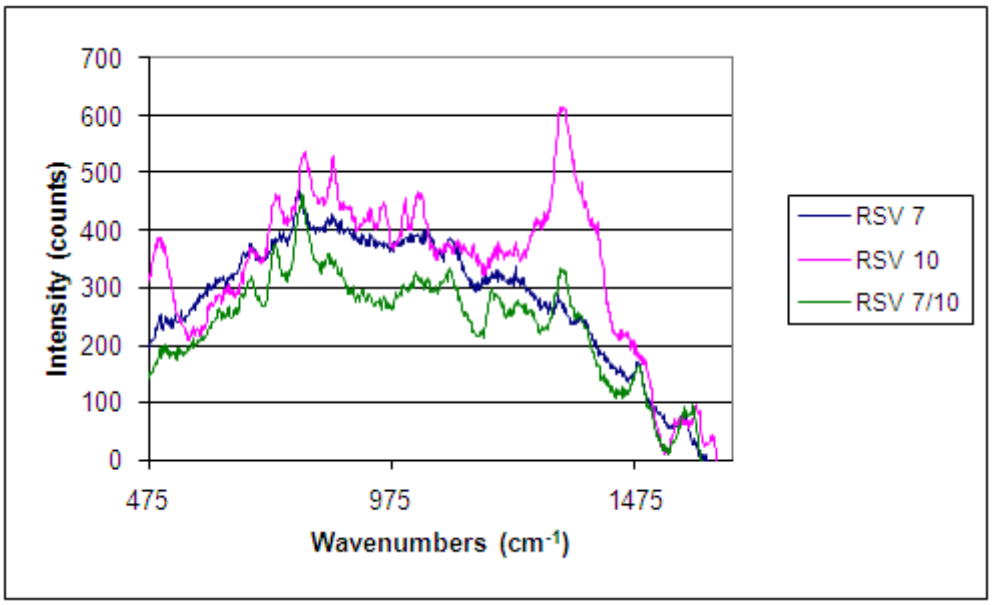

Figure C11: **Spectrum of RSV 7 and RSV 10 mixture with RSV 7 and RSV 10 Spectra in Nanopure Water.**

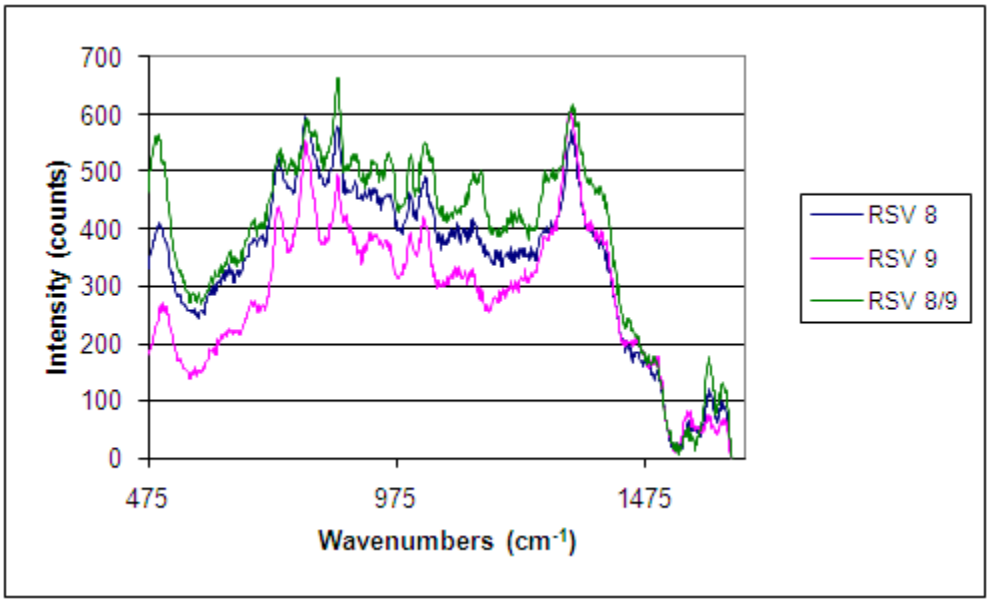

Figure C12: **Spectrum of RSV 8 and RSV 9 mixture with RSV 8 and RSV 9 Spectra in Nanopure Water.**